RNAi experiments, purified adenovirus, which directs synthesis of siRNA *in vivo*, was applied to cultured neural tubes for 6 h and then the explants were used for the stripe assay.

In ovo RNAi of chick embryo

Embryos obtained from fertilized chicken eggs (Takeuchi Farm Inc.) were staged according to the Hamburger and Hamilton method. For tracing of NCCs lacking specific target proteins in the developing chick embryos, cPlexin-A2 RNAi plasmid, cNeuropilin-1 RNAi plasmid, or cPlexin-D1 RNAi plasmid were electroporated into chick embryos stage 9 *in ovo* using an electroporator (CUY-21, BEX Co.). Briefly, tungsten needles, serving as anode and cathode electrodes, were placed on either side of the neuroepithelium. Concurrent with the injection of the solution containing RNAi plasmid (40 pmol/ml) into the neural tube with a sharp glass pipette, three electric pulses were applied (25 V, 50 ms). Eggs were shielded and allowed to develop up to HH stage 20. At 48 h post-electroporation, embryos were removed and fixed. GFP-positive cells in whole-mount embryos were visualized under fluorescence microscopy and sectioned for immunohistochemistry.

Cell implantation

Embryos were incubated until stage 9. The eggs were windowed, the vitelline membrane was removed, and an incision was made between neural tube and the surrounding tissue from the mid-optic placode to the 3rd somite (corresponding to r6 to r8). HEK293 cells expressing Sema3C, Sema6A, or Sema6B were pelleted and pushed into position. Eggs were sealed and incubated for up to 24 h.

Corrosion casting

Corrosion casting was performed (Polysciences). Briefly, heterozygotes and homozygotes of Plexin-A2$^{-/-}$ mice at P0 were anesthetized with ketamine and perfused with PBS through the left ventricle after a small hole was introduced into the right atrium. A 1 ml tuberclin syringe was used to inject polymer into the left ventricle under gentle pressure. After perfusion with the polymer, the resin was left overnight to harden. After the mass had fully cured, the tissue surrounding the cast was corroded away by using Maceration Solution (Polysciences) at 50 °C.

In situ hybridization and immunohistochemistry

Whole-mount *in situ* hybridization analyses of mouse and chick embryos were performed as described (Nieto et al., 1996). The following RNA probes were used for *in situ* hybridization: cNeuropilin-1, cPlexin-A2, mPlexin-A2, cPlexin-D1, cRhoB, cSema3C, cSema6A, or cSema6B. RNA transcripts were synthesized using a digoxigenin (DIG)-labeling kit (Roche Mannheim) according to the manufacturer's protocol.

Immunohistochemistry was performed on whole-mount and cryosections of embryonic tissue. The following antibodies were used: the mouse anti-GFP IgG antibody (Santa Cruz), the mouse anti-HNK-1 IgM antibody (Zymed), and the mouse anti-myosin heavy chain IgG antibody (Sigma); and secondary antibodies anti-mouse IgG-FITC and anti-mouse IgM-Rhodamine.

Results

Semaphorin receptor expression in migrating cardiac NCCs

To determine the potential semaphorins and cognate receptors that may be involved in cardiac NCC formation, we first used RT-PCR to identify any migrating NCC semaphorin receptor with an increased mRNA level. A length of neural tube extending from the mid-optic placode to the 3rd somite (corresponding to r6 to r8), where cardiac NCCs migrate and contribute to the cardiac outflow tract formation, was dissected from the HH stage 10–11 chick embryos, and then cultured for two days *in vitro* until the robust migration of NCCs occurred. mRNA expression of chicken Pexin-A1, A2, A4, B1, B2 and D1, and neuropilin-1 and 2, which have been identified as chicken homologues to mammalian plexins and neuropilins, was compared between the neural tube and NCCs by RT-PCR (Fig. S1). Only Plexin-A2, Plexin-D1, and neuropilin-1 expression was increased in NCCs. We therefore focused on these receptors for further analysis.

The expression of these molecules was analyzed *in vivo* by *in situ* hybridization at Hamburger–Hamilton (HH) stages 10 and 20, when cardiac NCCs delaminate from the neural tube and arrive at the cardiac outflow tract, respectively (Martinsen, 2005) (Fig. 1). Plexin-A2 mRNA was detected in a stream of cells beginning at the dorsal neural tube (Fig. 1A) which is consistent with the expression pattern of RhoB mRNA. As RhoB mRNA is an early marker for NCCs (Perez-Alcala et al., 2004) (Fig. 1B), it is likely that Plexin-A2 is also expressed in NCCs. Subsequently, Plexin-A2 mRNA expression became prominent in the surrounding tissue at the third and fourth through sixth pharyngeal arch arteries and in the mesenchymal tissue at the cardiac outflow tract (Figs. 1C and D). On the other hand, neither Plexin-D1 nor neuropilin-1 were detected in the NCCs at the stage 10. At stage 20, Plexin-D1 expression became prominent in the endothelial cells of the pharyngeal arch arteries and in endocardial and mesenchymal cells of the cardiac outflow tract (Figs. 1E and F). Neuropilin-1 became prominent in the dorsal root ganglion, the endothelial cells of vessels including the pharyngeal arch arteries, and the endocardial and mesenchymal cells of the cardiac outflow tract (Figs. 1G and H). In addition, Plexin-A2, Plexin-D1 and neuropilin-1 expressions (Figs. 1I–N) exhibited a similar distribution of the neural crest cell marker HNK-1 beside neural tube (Figs. 1I′, K′ and M′) and in the mesenchyme of cardiac outflow tract (Figs. 1J′, L′ and N′), suggesting that NCCs express Plexin-A2, Plexin-D1 and neuropilin-1 mRNAs during migration. These expression patterns of Plexin-A2, Plexin-D1 and Neuropilin-1 in chick embryos appeared to be similar to those observed in mouse embryos (Brown et al., 2001; Gitler et al., 2004; Kawasaki et al., 1999). Thus, the expression pattern of Plexin-A2, Plexin-D1 and neuropilins-1 implicates the role of each receptor in cardiac NCC migration.

Semaphorin receptor ligand identification and expression during cardiac neural crest development

Several studies in vertebrates have shown that type A plexins serve as direct receptors for class 6 semaphorins (Toyofuku et al., 2004a; Suto et al., 2005), and in *Drosophila*, Plexin-A serves as a direct receptor for class 6-related Sema-1a (Winberg et al., 1998). Alkaline Phosphatase (AP)-conjugated Sema6A (AP-Sema6A) specifically binds to cells expressing Plexin-A2 and -A4 (Suto et al., 2007), and AP-Sema3C exhibits the strong binding to neuropilins-1/Plexin-D1 heterodimer, the weak binding to neuropilins-1 alone or neuropilins-1/Plexin-A1 heterodimer, and the weakest binding to Plexin-A1 or Plexin-D1 alone (Gitler et al., 2004). Consistent with their results, our binding experiment together with the colorimetric analysis of bound AP demonstrated a direct binding of AP-Sema6B as well as AP-Sema6A to cells expressing Plexin-A2 and the binding of AP-Sema3C to cells expressing both Plexin-D1 and NP1 and the weak binding to neuropilins-1 alone or neuropilins-1/Plexin-A2 heterodimer (Figs. 2A and B).

The expression of Sema6A, 6B, and 3C was analyzed *in vivo* by *in situ* hybridization at Hamburger–Hamilton (HH) stages 10 and 20 (Figs. 1O–X). At stage 10, Sema6A and Sema6B mRNA expression was first detected in the somite and the dorsal side of neural tube, respectively (Figs. 1O and P). At stage 20, the distribution of Sema6A mRNA was detected in dorsal side of neural tube, myotome and lateral ectoderm (Figs. 1Q and R). Sema6B mRNA expression was detected in dorsal root ganglion, the dorsal side of neural tube and the myotome

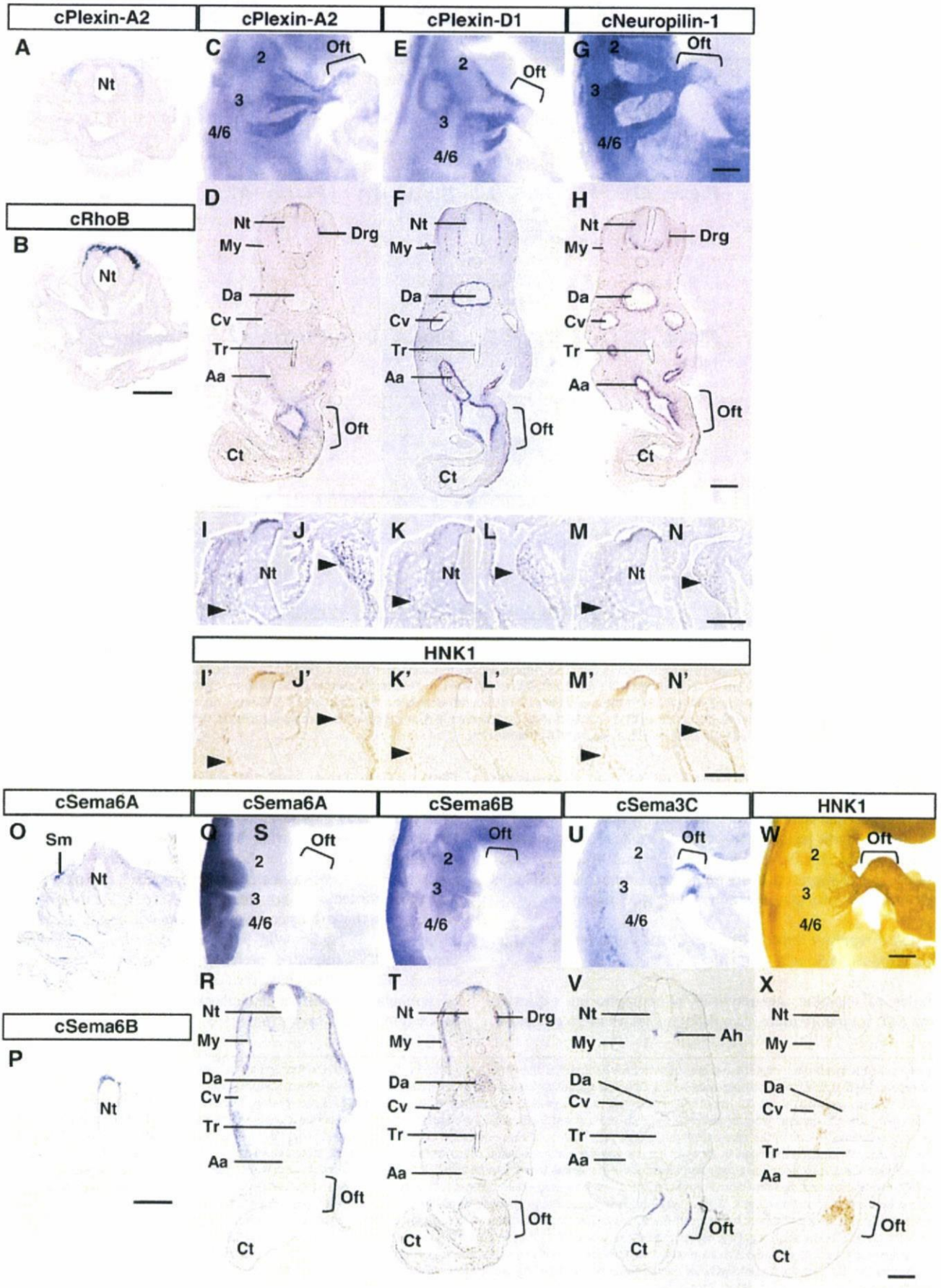
cPlexin-A2
cPlexin-A2
cPlexin-D1
cNeuropilin-1
A
Nt
C
2
3
4/6
Oft
E
2
3
4/6
Oft
G
2
3
4/6
Oft
cRhoB
B
Nt
D
Nt
My
Drg
Da
Cv
Tr
Aa
Oft
Ct
F
Nt
My
Da
Cv
Tr
Aa
Oft
Ct
H
Nt
My
Drg
Da
Cv
Tr
Aa
Oft
Ct
I
J
K
L
M
N
Nt
HNK1
I'
J'
K'
L'
M'
N'
cSema6A
cSema6A
cSema6B
cSema3C
HNK1
O
Sm
Nt
Q
S
2
3
4/6
Oft
U
2
3
4/6
Oft
W
2
3
4/6
Oft
cSema6B
P
Nt
R
Nt
My
Da
Cv
Tr
Aa
Oft
Ct
T
Nt
Drg
My
Da
Cv
Tr
Aa
Oft
Ct
V
Nt
My
Ah
Da
Cv
Tr
Aa
Oft
Ct
X
Nt
My
Da
Cv
Tr
Aa
Oft
Ct

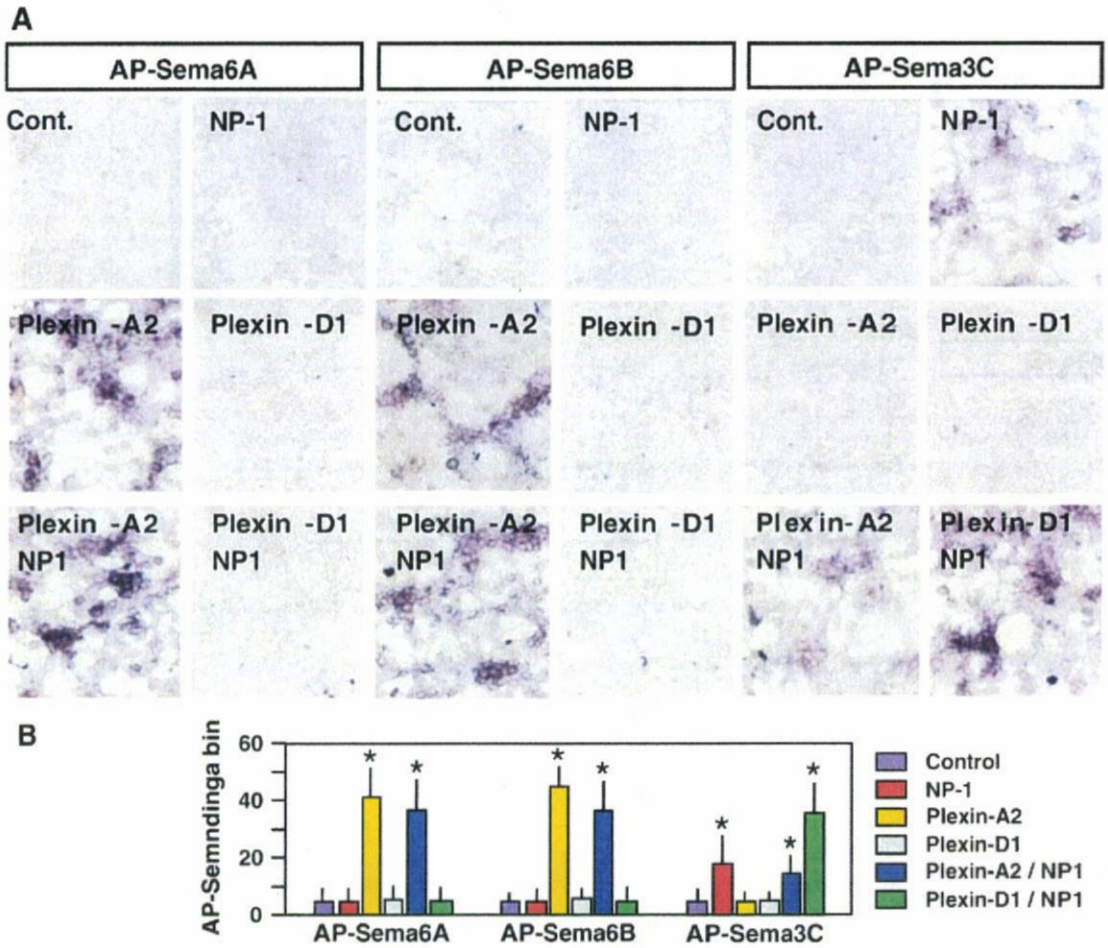

Fig. 2. Identification of semaphorin ligands and their expression in the chick embryo. (A) Micrographs of binding assays that test for the binding of AP-Sema6A, AP-Sema6B, or AP-Sema3C on HEK293 cells transfected with vectors containing Plexin-A2, Plexin-D1, Neuropilin-1, or their combinations. By using alkaline phosphatase substrates, a strong binding of AP-Sema6A or AP-Sema6B to Plexin-A2 and AP-Sema3C to Neuropilin-1/Plexin-D1 heterodimer, while a weak binding of AP-Sema3C to neuropilins-1 or neuropilins-1/Plexin-A2 heterodimer were detected. Scale bar, 50 μm. (B) Summary of AP-sema binding experiments of four experiments with similar results. Data are displayed as mean pixel intensity (arbitrary units) after subtraction of background (mean±SEM, $n=4$). *$p<0.01$ from control.

(Figs. 1S and T). On the other hand, Sema3C mRNA expression was not detected at the stage 10 but then was prominent in the anterior horn cells, and the muscular layer of the cardiac outflow tract at the stage 20 (Figs. 1U and V). In this region, HNK-positive cardiac NCCs lie adjacent to the territory of Sema3C mRNA (Figs. 1W and X). Thus, these expression patterns suggest that the interaction between semaphorins and their receptors may play a role in cardiac NCC migration.

NCCs exhibit a repulsive response to both Sema6A and Sema6B but an attractive response to Sema3C

In order to examine the activities of semaphorins expressed along the NCC migratory route, two different assays were employed. First, NCCs isolated from HH stage 10 embryos were placed on alternating stripes consisting of either the semaphorin–Fc chimeric protein (30 nM) plus fibronectin or fibronectin alone to determine the effect of semaphorins on the *in vitro* migration of NCCs. Although the NCCs did not display any preference in their migration behaviors between stripes containing control IgG plus fibronectin and those containing fibronectin alone (Fig. 3A), a majority of NCCs migrated on the stripes containing fibronectin alone and avoided the stripes containing Sema6A–Fc or Sema6B–Fc (Figs. 3B and C). In contrast, NCCs migrated preferentially on the stripes containing Sema3C–Fc (Fig. 3D). These results also indicate that the ectodomain of semaphorins such as semaphorin–Fc protein is involved in the regulation of NCC migration.

Fig. 1. Expression of semaphorin receptors and semaphorin ligands in chick embryos. (A–N) cPlaxin-A2, cPlexin-D1, cNeuropilin-1 and cRhoB expression were analyzed by either transverse section (A, B, D, F, H, I–N) or whole-mount (C, E, G) *in situ* hybridization and HNK-1 expression were analyzed by immunostaining (I′–N′). (A, B) In HH stage 10, cPlexin-A2 is expressed in regions lateral to the dorsal side of neural tube (Nt) and in a pattern that resembles that of cRhoB. (C–H) In HH stage 20, cPlexin-A2 expression is detected in the dorsal root ganglion (Drg) and the mesenchyme surrounding the 2nd, 3rd and 4–6th pharyngeal arch arteries (2, 3, 4/6) and extends into the mesenchyme of the outflow tract (Oft) (C, D). cPlexin-D1 expression is detected in the pharyngeal arch arteries (2, 3, 4/6) and the endothelial cells of aortic arteries (Aa, Da), and endocardial cells in the Oft (E, F). cNeuropilin-1 expression overlaps cPlexin-D1 expression in Drg and the endothelial and endocardial cells but is also seen in the tissue surrounding vessels and mesenchyme of the Oft (G, H). cPLexin-A2, cPlexin-D1 and cNeuropilin-1 expressions (arrowheads) are detected in migrating NCCs besides neural tube (I, K, M) and in the mesenchyme of Oft (J, L, N). (I′–N′) Migrating NCCs were visualized by immunostaining with anti-HNK-1 antibody in sections adjust to panels I to N, respectively. (O–V) cSema6A, cSema6B and cSema3C expression were analyzed by transverse section (O, P, R, T, V) or whole-mount (Q, S, U) *in situ* hybridization. (O, P) In HH stage 10, cSema6A and cSema6B expression are detected in the somite (Sm) and the dorsal side of neural tube (Nt), respectively. (Q–V) In HH stage 20, cSema6A expression is also prominent in dorsal side of Nt and myotome (My) and lateral side of ectoderm (Q, R), cSema6B expression is in Drg, My, and the dorsal side of Nt (S, T), and cSema3C expression is in the anterior horn cells (Ah) and myocardial layer of Oft (U, V). (W, X) NCCs were immunostained with an anti-HNK-1 antibody in whole-mount (W) and in transverse sections (X). NCCs migrate in a stream medial to My through the tissue surrounding the aortic arteries (Aa, Da) into the mesenchyme of the Oft. Scale bar, 100 μm. Aa, aortic artery; Cv, cardinal vein; Ct, cardiac tube; Da, dorsal aorta; Drg, dorsal root ganglion; My, myotome; Nt, neural tube; Oft, outflow tract; Tr, trachea.

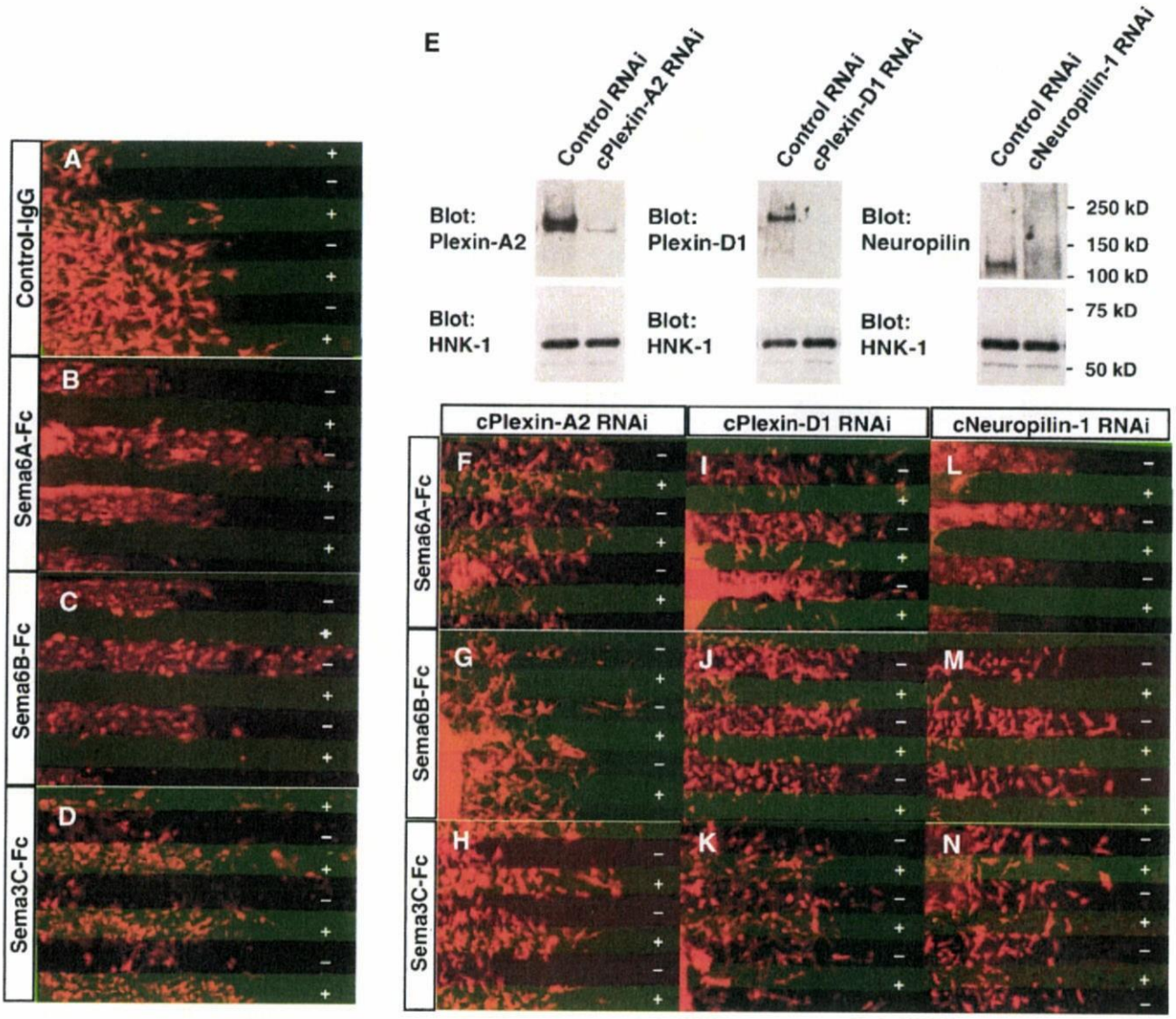

Fig. 3. Repulsive response to Sema6A and Sema6B through Plexin-A2 and an attractive response to Sema3C through Plexin-D1 and Neuropilin-1 in NCCs. (A–D) Migration of NCCs on stripes containing Sema6A–Fc, Sema6B–Fc, or Sema3C–Fc. Neural tube explants derived from rhombomere regions r6 to r8 were cultured on a substratum composed of alternating stripes of Sema6A–Fc, Sema6B–Fc, or Sema3C–Fc/fibronectin and FITC-labeled BSA (+) versus fibronectin alone (−). After 2 days, cultures were fixed and stained with an anti-HNK-1 antibody to visualize NCCs. NCCs avoided stripes containing Sema6A–Fc and Sema6B–Fc, whereas NCCs remained on stripes containing Sema3C–Fc. In control experiments in which NCCs cultured on a substratum composed of alternating stripes of human IgG/fibronectin (+) versus fibronectin alone (−), NCCs showed no preference in their migratory patterns on the control substratum. Scale bar, 100 μm. (E) Efficiency and specificity of RNAi for cPlexin-A2, cPlexin-D1, or cNeuropilin-1. Immunoblot analysis using NCCs infected with RNAi adenovirus show the specific suppression of target proteins. None of the RNAi adenovirus showed any obvious effect on HNK-1 expression. (F–N) Migration of NCCs lacking cPlexin-A2, cPlexin-D1, or cNeuropilin-1 on stripes consisting of Sema6A–Fc, Sema6B–Fc or Sema3C–Fc. Neural tube explants derived from hindbrain regions were infected with an RNAi adenovirus, and infected explants were cultured on a substratum composed of alternating stripes of Sema6A–Fc, Sema6B–Fc or Sema3C–Fc/fibronectin and FITC-labeled BSA (+) versus fibronectin alone (−). After 2 days, cultures were fixed and stained with an anti-HNK-1 antibody. NCCs infected with cPlexin-A2 adenovirus show attraction to Sema3C–Fc but loss of repulsion to Sema6A–Fc or Sema6B–Fc in their migratory pattern (F–H), whereas NCCs infected with either cPlexin-D1 RNAi adenovirus or cNeuropilin-1 RNAi adenovirus show a repulsion to Sema6A–Fc or to Sema6B–Fc but loss-of-attraction to Sema3C–Fc (I–N).

Furthermore, the NCC responsiveness to each semaphorin was examined by this stripe assay using a neural tube infected with shRNA synthesizing adenovirus against selected target mRNA (RNAi adenovirus). These RNAi adenoviruses efficiently and specifically suppressed target mRNA and protein (Fig. 3E and Fig. S2). When Plexin-A2 expression in NCCs was knocked down by such adenovirus infection, NCCs no longer avoided stripes containing Sema6A–Fc or Sema6B–Fc but demonstrated preference for stripes containing Sema3C–Fc (Figs. 3F–H). In contrast, shRNA-mediated knockdown of either neuropilin-1 or Plexin-D1 suppressed an attractive response of NCCs to Sema3C–Fc without affecting a chemorepulsive response to Sema6A or Sema6B (Figs. 3I–N). Thus, the NCC migratory behavior to each semaphorin was determined by the corresponding receptor.

Second, we also examined the guidance activities of semaphorins on NCC migration *in vivo* by implanting semaphorin-expressing cells to ectopic positions in the HH stage 10 chick embryo. Surface biotinylation-chase experiment showed the progressive decrease in full-length (150 kD) of Sema6A and Sema6B in the membrane fraction, in parallel with the increase in cleaved extracellular region (100 kD) of these semaphorins in the supernatant (Fig. 4A), indicating that Sema6A and Sema6B are released from the cell surface. Thus, Sema6A and Sema6B expressed in HEK293 cells probably exerts their activities as locally released soluble proteins and as membrane-bound proteins. Embryos receiving cell implants were sectioned and examined by immunohistochemistry using an anti-HNK-1 antibody (HH stage 20) (Figs. 4B–E). To quantitatively analyze the effect of semaphorin expressed in cells on

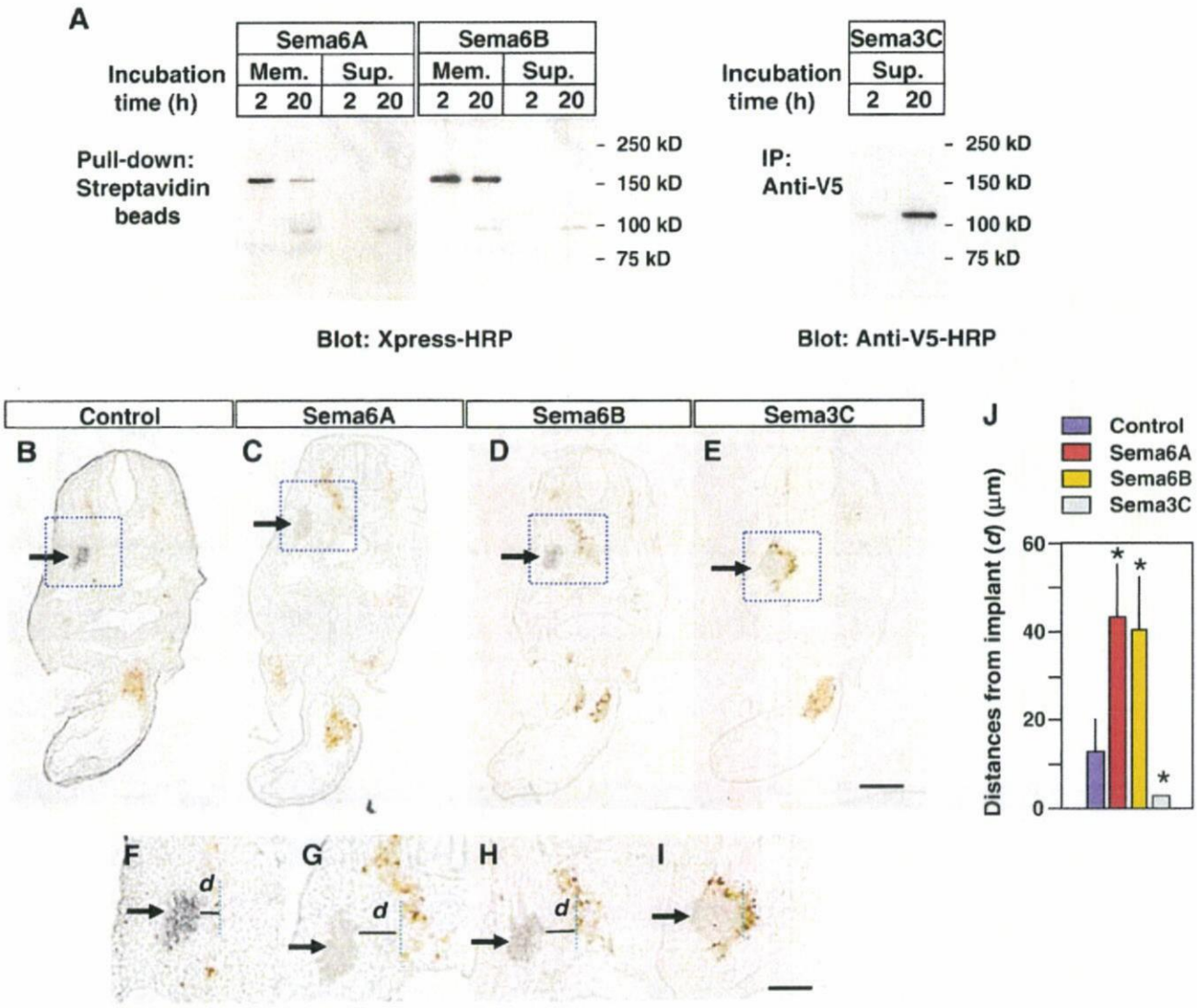

Fig. 4. The ectopic expression of Sema6A and Sema6B repels migrating NCCs but that of Sema3C attracts them in chick embryos. (A) Release of a soluble form of Sema6A, Sema6B, and Sema3C from the cell surface. Sema6A or Sema6B expressed in HEK293 cells were surface-labeled with biotin so that the full-length and the extracellular region of these semaphorins were pull-downed with streptavidin. Immunoblotting of immunoprecipitates using anti-Xpress-HRP shows the full-length (150 kDa) and the cleaved extracellular region (100 kDa) of Sema6A and Sema6B. Note the 100 kDa bands in the membrane fraction and supernatant with increased intensity during incubation, indicating that soluble forms of Sema6A and Sema6B are cleaved from membrane. Sema3C were immunoprecipitated from supernatants with an anti-V5 antibody and immunoblotting of immunoprecipitates using anti-V5-HRP shows the soluble full-length Sema3C (110 kDa). (B–E) Migration of NCCs in embryos that receives an ectopic source of Sema6A, Sema6B, or Sema3C. HEK293 cells expressing Sema6A, Sema6B, or Sema3C were stained with DiI and implanted into lateral side of trunk from r6 to r8 of the chick embryos at HH stage 10. The distribution of HNK-1-positive NCCs was analyzed at HH stage 20. The positions of the DiI-positive implants are indicated by arrows. Note the aberrant position of HNK-1-positive NCCs in embryos that received Sema6A, Sema6B-expressing cells and accumulation of cells close to implant in embryo that received Sema3C-expressing cells. Scale bar, 100 μm. (F–I) Distances between the implant and NCCs around implant were measured as shown in the figure. Scale bar, 50 μm. (J) Summary of distances between implant and NCCs of four experiments with similar results. Data are displayed as mean ±SEM (n=4). *p<0.01 from control.

the NCC migration, we measured the distance between the edge of implant and NCC cells around implant (Figs. 4F–J). Compared with control implants (Figs. 4B, F and J), implants of either Sema6A- or Sema6B-expressing cells resulted in skewed NCC migrations. That is, NCCs steered around the Sema6A- or Sema6B-rich regions encircling the implanted cells (Figs. 4C, D, G, H and J). On the other hand, many NCCs were attracted to and accumulated around the Sema3C-expressing implants (Figs. 4E, I and J). These results indicate that NCCs exhibit two different semaphorin type-specific responses: repulsion to Sema6A or Sema6B and attraction to Sema3C.

NCCs lacking semaphorin receptors lost their ability to migrate into the cardiac outflow tract

To investigate whether semaphorin signals are necessary for NCC navigation to the cardiac outflow tract *in vivo*, we knocked down the expression of cPlexin-A2, cPlexin-D1 or cNeuropilin-1 of neural cells in the neural tube before the robust migration of NCCs occurred in this region. This knock down was achieved by electroporating the pRNAT-H1.1/shuttle plasmid (RNAi plasmid) encoding shRNA and GFP into the right side of the neural tube in the stage 9 chick embryos. shRNAs synthesized by RNAi plasmid successfully suppressed the target mRNA and protein levels, when their RNAi constructs were cloned into adenovirus and transduced in NCCs (Fig. 3A and Fig. S2). At 48 h post-electroporation with RNAi plasmid, electroporated embryos were sectioned and immunostained with an anti-HNK-1 antibidy (Figs. 5E–H). A majority of HNK-1-positive cells migrating from neural tube coexpressed GFP (Figs. 5I–L), indicating that NCCs are successfully electroporated with RNAi plasmid. GFP-positive cells that expressed control shRNA could migrate normally into the cardiac outflow tract (Figs. 5A and E). When Plexin-A2 expression was knocked down, most of the GFP-positive cells lingered in the dorsal

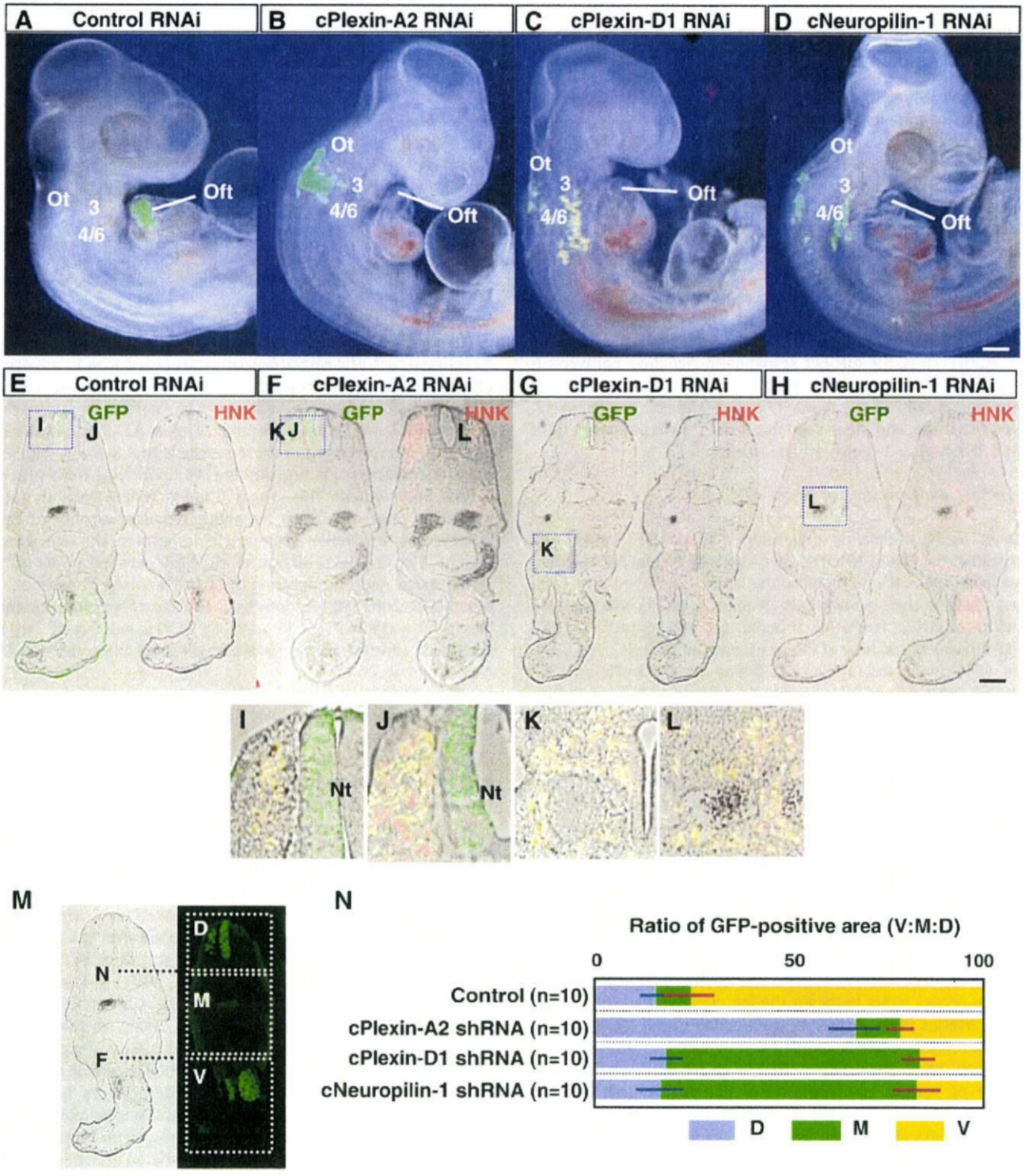

Fig. 5. Distribution of NCCs lacking cPlexin-A2, cPlexin-D1 or cNeuropilin-1 in chick embryo. After electroporation of RNAi plasmid into the right-side of the neural tube at r2 to 8 of HH stage 10 embryo, the distribution of GFP-positive NCCs (green) in HH stage 19–22 chick embryos were detected by fluorescence microscopy (A–D) or by immunohistochemistry on transverse sections with an anti-GFP antibody (green) and an anti-HNK-1 antibody (red) (E–H and high power shown in panels I–L). Note that a majority of cells migrating from neural tube (Nt) show the overlap of GFP-positive labeling with HNK-1-positive labeling (I–L). (A, E, I) Migrating NCCs electroporated with control RNAi plasmid reside in their characteristic positions. (B, F, J) Migrating NCCs electroporated with cPlexin-A2 RNAi plasmid distribute in regions dorsal–lateral to the neural tube, but not in the cardiac outflow tract (Oft). (C, G, K) Migrating NCCs electroporated with cPlexin-D1 RNAi plasmid diffusely distribute in the longitudinal and transverse axes without in the cardiac outflow tract (D, H, L) Migrating NCCs electroporated with cNeuropilin-1 RNAi plasmid diffusely distribute in a similar pattern to that of cPlexin-D1. Numbers in panels A–D indicate the number of pharyngeal arches. Ot, otic vesicle. (M). Localization of GFP-positive NCCs into three domains defined therein: dorsal domain (D), middle (M), and ventral (V). N, notochord; F, ventral endoderm of foregut. (N) Quantification of the numbers of GFP-positive NCCs located in distinct domains of chick embryo. In the dorsal domain, GFP-positive cells in neural tube were estimated as neuroepithelial cells instead of NCCs and were omitted. Data in each domain obtained from 10 experiments are summarized as a percentage of the total GFP-positive NCCs. Horizontal bar indicates SEM. Scale bar, 100 μm.

region and failed to egress from the area where Sema6A and Sema6B were expressed (Figs. 5B and F). The GFP-positive cells with suppressed Plexin-D1 expression distributed diffusely in the longitudinal-transverse axes instead of entering the cardiac outflow tract, even though they still migrated out from the dorsal region (Figs. 5C and G). A similar distribution of GFP-positive cells was observed when cNeuropilin-1 expression was suppressed (Figs. 5D and H).

In order to estimate the distribution of the migratory population, serial sections of some of the electroporated embryos were analyzed by measuring the area occupied by GFP-positive cells. Transverse sections of embryo were visually divided into three domains (dorsal, middle, and ventral), and the number of GFP-positive cells in each domain was counted (Fig. 5I). Compared to the experiments using a control RNAi plasmid (D:M:V=14: 9: 77), the experiments using a cPlexin-A2 RNAi plasmid exhibited the retardation of migratory cells in the dorsal side of trunk (D:M:V=64: 13: 23) and the experiments using a cPlexin-D1 RNAi plasmid or cNeuropilin-1 RNAi plasmid exhibited the diffuse distribution in the pharyngeal arches (D:M:V=18: 62: 20 for cPlexin-D1 RNAi and 15: 64: 21 for cNeuropilin-1 RNAi) (Fig. 5J). Thus, the distinct semaphorin signaling pathways is required for the correct pathfinding of NCCs. The departure of NCCs from the dorsal side of the trunk is dependent on the Plexin-A2-mediated repulsion, and the destination of NCCs is dependent on the Plexin-D1/Neuropilin-1-mediated attraction.

Cardiovascular malformations of Plexin-A2$^{-/-}$ mice

Suto et al. have recently generated a Plexin-A2$^{-/-}$ allele and demonstrated that Plexin-A2, in cooperation with Plexin-A4, and their putative ligand Sema6A, all regulate the lamina-restricted projection of mossy fibers in the hippocampus (Suto et al., 2007). We analyzed the binding of AP–Sema6A, AP–Sema6B, and AP–Sema3C to NCCs derived from the neural tube of Plexin-A2 mutant mice (Fig. 6A). AP–Sema6A, AP–Sema6B and AP–Sema3C bound to NCCs in Plexin-A2$^{+/-}$ mice, but AP–Sema6A and AP–Sema6B did not bind to NCCs in Plexin-A2$^{-/-}$ mice. This finding also confirmed that mouse embryo NCCs respond to Sema6A and Sema6B through Plexin-A2. We next analyzed offspring from intercrosses of heterozygous mice. In 8 out of 13 Plexin-A2$^{-/-}$ mice at E12.5, transverse embryo sections exhibited structural defects in the cardiac outflow of the heart. Aortic and pulmonary channel septation (Fig. 6B), where Plexin-A2 is prominently expressed, was lacking (Fig. 6C, asterisk) (Brown et al., 2001). These results indicate that Plexin-A2 is involved in the cardiac outflow tract formation and probably through regulating cardiac NCC migration. In four out of 11 Plexin-A2$^{-/-}$ mice at P0, the cardiac phenotypes evaluated by cast corrosion exhibited cardiovascular malformations (Fig. 6D and Table 2). Incomplete septation of the conotruncus, known as persistent truncus arteriosus (PTA), was observed. In addition, this interruption occurs either between the left common carotid and left subclavian arteries (Type B interruption, middle panel of Fig. 6D) or between the branchiocephalic and left common carotid arteries (Type C interruption, right panel of Fig. 6D). Such locations indicate the disturbance of various combinations of pharyngeal arch arteries, including those derived from the third and fourth pharyngeal arches (Creazzo et al., 1998). Incomplete penetrance of the mutation is due to the partial NCC migration into the cardiac outflow tract in some fractions of Plexin-A2$^{-/-}$ mice. Immunohistochemistry using an anti-HNK-1 antibody showed less but some degree of HNK-1-positive cells in Plexin-A2$^{-/-}$ mice, compared with those in Plexin-A2$^{+/-}$ mice (Figs. 6E and F). Thus, there should be some compensatory mechanisms for the defects of NCC migration in Plexin-A2$^{-/-}$ mice.

Discussion

NCCs are generated from subsets of neuroepithelial cells through a sequential intrinsic program and obtain mesenchymal properties, most evidently, the capability to migrate to a specific target organ (the epithelial–mesenchymal transformation) (Gammill and Bronner-Fraser, 2003; Le Douarin et al., 2004). The polarized guidance response generated to a very shallow gradient of chemotactic molecules can be established by the asymmetric localization of intracellular signaling components (Charest and Firtel, 2006; Ridley et al., 2003). However, how long-range migrating cells such as NCCs achieve the precise pathfinding to a target organ remained unclear. Here, we show evidence that the polarized NCC guidance response is established by the coordination of contact repellents such as transmembrane class 6 semaphorins expressed along the migratory routes as well as by diffusible attractants such as class 3 semaphorins at the target tissue.

Sema6A and Sema6B initiate NCC migration from dorsal neural tube through Plexin-A2

Cardiac NCC pathfinding requires segmented and dorso-ventral directional cues. The migratory pathway of cardiac NCCs appears to be demarcated by the territory provided by Sema6A and Sema6B. Both *in vitro* and *in vivo* analyses reveal that NCCs exhibit a repulsive response to Sema6A and Sema6B through Plexin-A2. The plausible and attractive interpretation of these results is that Sema6A and Sema6B work as contact repellents, pushing the underlying NCCs toward the cardiac outflow tract. This proposed function of Sema6A and Sema6B would be consistent with the chemorepellent activity of Sema6A observed in cerebellar granule cell migration through Plexin-A2 (Leighton et al., 2001; Kerjan et al., 2005; Renaud et al., 2008), in spinal motor neuron migration through Plexin-A2 (Bron et al., 2007; Mauti et al., 2007) and in hypothalamic mossy fiber extension through Plexin-A2 and Plexin-A4 (Suto et al., 2007), and that of Sema6B in peripheral sensory and sympathetic ganglion axons through Plexin-A4 (Suto et al., 2005).

The molecular mechanism of semaphorin-mediated growth cone collapse has been extensively investigated. However, how semaphorin–plexin signaling controls cell migration is still unclear. It is likely that Sema6A/Sema6B–Plexin-A2 signaling moderates cell migration through controlling the cell–cell and/or cell–matrix adhesion. Secreted class 3 semaphorins, by binding to neuropilin and to the type A plexin complex, exert their repulsive activity via the suppression of integrin-mediated cell adhesion (Serini et al., 2003; Toyofuku et al., 2005; Banu et al., 2006). *Drosophila* Sema1a, an invertebrate orthologue of class 6 semaphorins, facilitates motor axon defasciculation at the neuromuscular junction by countering the homophilic adhesion of fasciculin II protein (Yu et al., 2000) and ensures class-specific olfactory axon segregation by counting the adhesion of N-cadherin (Lattemann et al., 2007). In fact, cranial NCC motility is regulated by the integrin-mediated cell adhesion on surrounding tissues (Strachan and Condic, 2004). Alternatively, recent study has demonstrated that Sema6A–Plexin-A2 signaling controls centrosome positioning in migrating cerebellar granule cells (Renaud et al., 2008). In migrating neurons, microtubules linked to the centrosome pull the nucleus during migration, thereby positioning nucleus toward the leading process. Thus, actin and microtubule dynamics involved in the semaphorin-mediated growth cone collapse may regulate cell migration of NCCs through controlling centrosome positioning. Furthermore, our study demonstrated that the extracellular region of Sema6A and Sema6B can be cleaved and function as locally diffused repellents. If it is the case *in vivo*, cells responsive to these semaphorins such as NCCs and cerebellar granule cells could migrate along the concentration gradient of released repellents. Altogether, class 6 semaphorins such as Sema6A and Sema6B could function as NCC releasing molecules, thereby facilitating their delamination from the neural tube and their migration from the dorsal region.

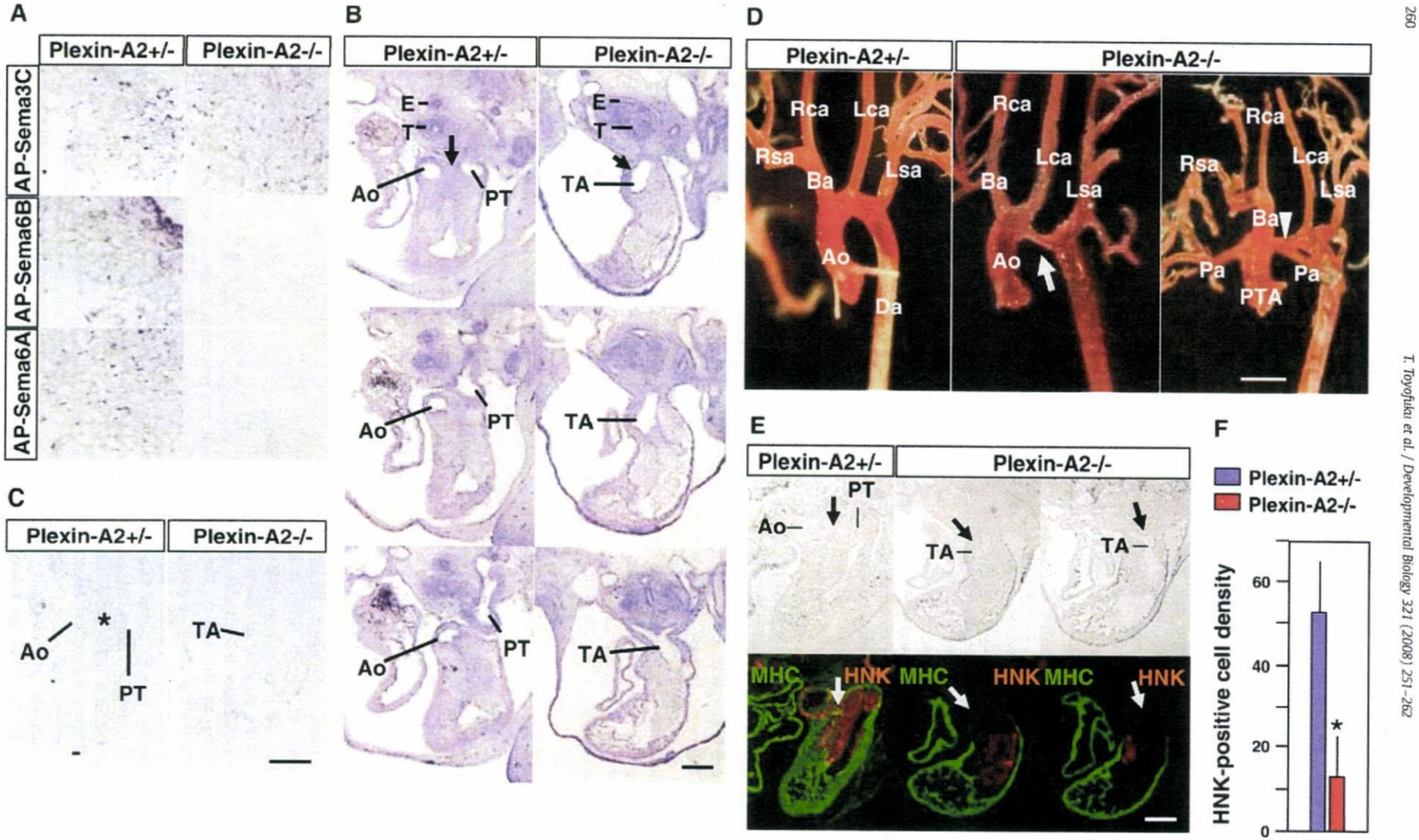

Fig. 6. Cardiovascular phenotype of Plexin-A2 mutant mice. (A) Micrographs of binding assays that test the binding of AP-Sema6A, AP-Sema6B, or AP-Sema3C on NCCs derived from Plexin-A2 mutant mice at E12.5. By using alkaline phosphatase (AP) substrates, significant staining was observed between AP-Sema6A, AP-Sema6B, or AP-Sema3C and NCCs derived from Plexin-A2$^{+/-}$ mice, and between AP-Sema3C and NCCs from Plexin-A2$^{-/-}$ mice. Scale bar, 50 μm. (B) Histology of sequential transverse sections through the aortic sac (Top to bottom) in Plexin-A2$^{+/-}$ mice (left panels) and Plexin-A2$^{-/-}$ mice (right panels) at E11.5. Arrows indicate the sites where the aorticopulmonary septum normally forms and which have a high percentage of neural crest-derived cells. Note a septation of the aortic and pulmonary channels of Plexin-A2$^{+/-}$ mice but a lack of septation in Plexin-A2$^{-/-}$ mice. Ao, aortic trunk; E, esophagus; PT, pulmonary trunk; T, trachea; TA, truncus arteiosus. (C) Transverse section *in situ* hybridization reveals Plexin-A2 expression restricted to the cardiac outflow tract (asterisk) in Plexin-A2$^{+/-}$ mice but not in Plexin-A2$^{-/-}$ mice. (D) The cardiovascular phenotype is characterized by corrosion casting. Methyl methacrylate was injected into the left ventricle of anesthetized P0 Plexin-A2 mutant mice. The cast of Plexin-A2$^{+/-}$ mice shows normal vascular architecture (left panel). Cast of Plexin-A2$^{-/-}$ mice shows the incomplete interruption of the aortic arch (Type B interruption, arrow) and with normal septation of the aortic and pulmonary trunks (middle panel). Another cast of Plexin-A2$^{-/-}$ mice shows persistent truncus arteriosus and interruption of the aortic arch (Type C interruption). The descending aorta has filled because the ductus arteriosus (arrowhead) has not closed completely. Ao, ascending aorta; Ba, branchiocephalic artery; Da, descending artery; E, esophagus; Lca, left common carotid artery; Lsa, left subclavian artery; Pa, pulmonary artery; PTA, persistent truncus arteriosus; Rca, Right common carotid artery; Rsa, Right subclavian artery; T, trachea. (E) Translucent (upper panels) and immunostained images (lower panels) with anti-myosin heavy chain (HMC; green) and anti-HNK-1 (HNK; red) antibodies on transverse sections through the septation of aortic arch and pulmonary trunk (arrows) in Plexin-A2 mutant mice. HNK-1-positive NCCs are distributed in the endocardial cushion of the cardiac outflow tract, and they are delineated from MHC-positive myocardial cells. Note the fewer but various amounts of HNK-positive NCCs in Plexin-A2$^{-/-}$ mice when compared with those in Plexin-A2$^{+/-}$ mice. Scale bar, 100 μm for panels A, B, C, and E, 250 μm for panel D. (F) Summary of HNK-1 positive cells in cardiac outflow tract shown in panel E. Data are displayed as mean pixel intensity (arbitrary units) after subtraction of background (mean ± SEM, $n=5$). *$p<0.01$ from Plexin-A2$^{+/-}$.

Sema3C attracts NCCs to the cardiac outflow tract through the Plexin-D1/Neuropilin-1 complex

After migrating through the dorso-lateral territory, cardiac NCCs reach their final target destinations and subsequently differentiate into endocardial and smooth muscle cells. Therefore, in addition to the necessity of Sema6A and Sema6B as an NCC egress from the dorso-lateral region, another guidance cue must be required for attracting to and accumulating NCCs at the target tissue. Our present study demonstrated that Sema3C functions as this attraction cue. The timing of Sema3C expression at the outflow tract region appears to coincide with that of NCC accumulation at the same region. In fact, migrating NCCs accumulate in the cardiac cushion of the cardiac outflow tract and are surrounded by the Sema3C-expressing myocardial layer. Furthermore, Sema3C attracts NCC migration *in vitro* as well as *in vivo*.

Individual class 3 semaphorins can function as both chemorepellents and chemoattractants, depending on the particular axon type examined (Fiore and Puschel, 2003; Fujisawa, 2004). Sema3C repels sympathetic axons (Chen et al., 1998; Takahashi et al., 1998) but attracts cortical neurons (Bagnard et al., 1998). There have been several reports that class 3 semaphorins convert attractive and repulsive responses in target cells. Levels of cGMP and cAMP in growth cones may determine the attractive and repulsive responses of rat dorsal root ganglion axons, respectively (Song et al., 1998). Furthermore, the functional difference of class 3 semaphorins may be dependent on their activity on integrin function. The repulsive activity of Sema3A on endothelial cells requires the suppression of integrin function (Serini et al., 2003), while the attractive activity of Sema3C on endothelial cells requires the activation of integrin function (Banu et al., 2006). Thus, the particular interactions of neuropilins and specific plexins may confer the specificity of growth cone responses to each class 3 semaphorin. Sema3C binds to neuropilins-1 with the higher affinity to the Neuropilins-1/Plexin-D1 heterodimer than the Neuropilins-1/Plexin-A2 heterodimer. Although it is not completely ruled out the possibility that Plexin-A2 function as a co-receptor for Sema3C-mediated signal, the stripe assay indicates that Sema3C-induced attraction is mainly mediated through the Neuropilin-1/Plexin-D1 heterodimers.

Defects of the cardiac outflow tract formation in semaphorin–plexin knockout mice

Plexin-A2$^{-/-}$ mice exhibited cardiovascular defects which could be caused by the abnormality of NCC-mediated cardiac outflow tract formation. In fact, the accumulation of NCCs in the cardiac outflow tract seen in Plexin-A2$^{-/-}$ mice appeared to be less than that in Plexin-A2$^{+/-}$ mice (Fig. 6E). Since NCCs from Plexin-A2$^{-/-}$ mice exhibited similar BrdU incorporation and apoptotic cell populations to those from Plexin-A2$^{+/-}$ mice (Fig. S3), the abnormal migratory behavior of NCCs observed in this study might contribute to cardiac outflow tract formation defects in Plexin-A2 mutant mice. It is unknown how some populations of NCCs still migrate into cardiac outflow tract in Plexin-A2$^{-/-}$ mice. Plexin-A4 expression, which is negligible in the cardiac outflow tract (Fig. S1), also binds directly to Sema6A and mediates repulsive activity on the mossy fiber projection (Suto et al., 2005). Since Plexin-A4 expression appeared to be upregulated in the cardiac outflow tract in Plexin-A2$^{-/-}$ mice (Fig. S4), Sema6A signal could be transmitted through Plexin-A4 in Plexin-A2$^{-/-}$ mice. In fact, Plexin-A2$^{-/-}$;Plexin-A4$^{-/-}$ mice exhibited incomplete septation of the truncus arteriosus at a higher ratio than Plexin-A2$^{-/-}$ mice at E 12.5 (data not shown), suggesting that defects in cardiac outflow tract in Plexin-A2$^{-/-}$ mice is rescued by the Plexin-A4. These results indicate that the low penetrance of the cardiovascular phenotype of Plexin-A2$^{-/-}$ mice is due to the compensatory mechanism through Plexin-A4 in NCCs.

Cardiovascular defects involving the cardiac outflow and the aortic arch have been described in Sema3C, Plexin-D1, and Neuropilin-1 knockout mice (Feiner et al., 2001; Gitler et al., 2004; Kawasaki et al., 1999). Binding experiments revealed that these gene products comprise a receptor-ligand paracrine signal pathway (Gitler et al., 2004 and this study). Reduced NCC accumulation in the cardiac outflow tract is observed in Sema3C$^{-/-}$ and Neuropilin-1$^{-/-}$ mice, but not in Plexin-D1$^{-/-}$ mice. Thus, cardiac defects in Plexin-D1$^{-/-}$ mice may be caused primarily by the dysfunction of other Plexin-D1-expressing endothelial cells, while the NCC migratory behavior could still be compensated by another plexin family member. In the chick embryo, NCCs lacking Plexin-D1 or Neuropilin-1 could egress from the dorsal neural tube and migrate close to the pharyngeal arches but fail to invade the cardiac outflow tract. As time-lapse analyses reveal the failure of NCCs lacking Neuropilin-1 to invade into pharyngeal arches (McLennan and Kulesa, 2007), cardiovascular defects in Sema3C and Neuropilin-1 knockout mice should similarly be caused by the failure of Sema3C-mediated NCC invasion into the cardiac outflow tract.

In conclusion

A key issue in guidance signaling is that migrating cells must achieve a polarized output. A sufficiently robust difference between the front and the back of the cells is required to facilitate migration. One way to achieve this difference is to amplify the initially subtle concentration gradient from one side of the cell to the other (Charest and Firtel, 2006; Ridley et al., 2003). In addition to an intrinsic gradient amplifier, our results demonstrated that long-range migrating cells such as the NCCs use a dynamic balance of attractants and repellents as an effective mechanism to increase guidance polarity. In the developing brain, specific classes of neuroblasts migrate over long ranges, and this neuroblast migration also depends on a dynamic balance of repulsive and attractive molecules (Murase and Horwitz, 2002; Wu et al., 1999; Liu and Rao, 2003). Our results therefore provide a broad implication for our understanding of signaling pathways in long-range cell migration during organogenesis.

Acknowledgments

This study was supported by research grants from the Ministry of Education, Culture, Sports, Science and Technology of Japan and the CREST program of JST (T. T., H.K., and A. K), the Program for Promotion of Fundamental Studies in Health Sciences of the National Institute of Biomedical Innovation (A. K.), and the Target Protein Research Program of the Japan Science and Technology Agency (T. T. and A. K.).

Appendix A. Supplementary data

Supplementary data associated with this article can be found, in the online version, at doi:10.1016/j.ydbio.2008.06.028.

References

Bagnard, D., et al., 1998. Semaphorins act as attractive and repulsive guidance signals during the development of cortical projections. Development 125, 5043–5053.
Banu, N., et al., 2006. Semaphorin 3C regulates endothelial cell function by increasing integrin activity. FASEB J. 20, 2150–2152. Epub 2006 Aug 29.
Bron, R., et al., 2007. Boundary cap cells constrain spinal motor neuron somal migration at motor exit points by a semaphorin-plexin mechanism. Neural. Develop. 2, 21.
Brown, C.B., et al., 2001. PlexinA2 and semaphorin signaling during cardiac neural crest development. Development 128, 3071–3080.
Charest, P.G., Firtel, R.A., 2006. Feedback signaling controls leading-edge formation during chemotaxis. Curr. Opin. Genet. Dev. 16 , 339–347. Epub 2006 Jun 27.
Chen, H., et al., 1998. Semaphorin-neuropilin interactions underlying sympathetic axon responses to class III semaphorins. Neuron 21, 1283–1290.
Creazzo, T.L., et al., 1998. Role of cardiac neural crest cells in cardiovascular development. Annu. Rev. Physiol. 60, 267–286.
Eickholt, B.J., et al., 1999. Evidence for collapsin-1 functioning in the control of neural crest migration in both trunk and hindbrain regions. Development 126, 2181–2189.

Epstein, J.A., et al., 2000. Migration of cardiac neural crest cells in Splotch embryos. Development 127, 1869–1878.
Etchevers, H.C., et al., 2001. The cephalic neural crest provides pericytes and smooth muscle cells to all blood vessels of the face and forebrain. Development 128, 1059–1068.
Feiner, L., et al., 2001. Targeted disruption of semaphorin 3C leads to persistent truncus arteriosus and aortic arch interruption. Development 128, 3061–3070.
Fiore, R., Puschel, A.W., 2003. The function of semaphorins during nervous system development. Front Biosci. 8, s484–s499.
Fujisawa, H., 2004. Discovery of semaphorin receptors, neuropilin and plexin, and their functions in neural development. J. Neurobiol. 59, 24–33.
Gammill, L.S., Bronner-Fraser, M., 2003. Neural crest specification: migrating into genomics. Nat. Rev. Neurosci. 4, 795–805.
Gammill, L.S., et al., 2006. Guidance of trunk neural crest migration requires neuropilin 2/semaphorin 3F signaling. Development 133, 99–106. Epub 2005 Nov 30.
Gitler, A.D., et al., 2004. PlexinD1 and semaphorin signaling are required in endothelial cells for cardiovascular development. Dev. Cell. 7, 107–116.
Gruber, P.J., Epstein, J.A., 2004. Development gone awry: congenital heart disease. Circ. Res. 94, 273–283.
Gu, C., et al., 2005. Semaphorin 3E and plexin-D1 control vascular pattern independently of neuropilins. Science 307, 265–268. Epub 2004 Nov 18.
Kawasaki, T., et al., 1999. A requirement for neuropilin-1 in embryonic vessel formation. Development 126, 4895–4902.
Kerjan, G., et al., 2005. The transmembrane semaphorin Sema6A controls cerebellar granule cell migration. Nat. Neurosci. 8, 1516–1524. Epub 2005 Oct 2.
Kirby, M.L., et al., 1983. Neural crest cells contribute to normal aorticopulmonary septation. Science 220, 1059–1061.
Krull, C.E., et al., 1997. Interactions of Eph-related receptors and ligands confer rostrocaudal pattern to trunk neural crest migration. Curr. Biol. 7, 571–580.
Lattemann, M., et al., 2007. Semaphorin-1a controls receptor neuron-specific axonal convergence in the primary olfactory center of Drosophila. Neuron 53, 169–184.
Le Douarin, N.M., et al., 2004. Neural crest cell plasticity and its limits. Development 131, 4637–4650.
Leighton, P.A., et al., 2001. Defining brain wiring patterns and mechanisms through gene trapping in mice. Nature 410, 174–179.
Liu, G., Rao, Y., 2003. Neuronal migration from the forebrain to the olfactory bulb requires a new attractant persistent in the olfactory bulb. J. Neurosci. 23, 6651–6659.
Martinsen, B.J., 2005. Reference guide to the stages of chick heart embryology. Dev. Dyn. 233, 1217–1237.
Mauti, O., et al., 2007. Semaphorin6A acts as a gate keeper between the central and the peripheral nervous system. Neural Develop. 2, 28.
McLennan, R., Kulesa, P.M., 2007. In vivo analysis reveals a critical role for neuropilin-1 in cranial neural crest cell migration in chick. Dev. Biol. 301, 227–239. Epub 2006 Aug 10.
Murase, S., Horwitz, A.F., 2002. Deleted in colorectal carcinoma and differentially expressed integrins mediate the directional migration of neural precursors in the rostral migratory stream. J. Neurosci. 22, 3568–3579.
Nieto, M.A., et al., 1996. In situ hybridization analysis of chick embryos in whole mount and tissue sections. Methods Cell Biol. 51, 219–235.
Osborne, N.J., et al., 2005. Semaphorin/neuropilin signaling influences the positioning of migratory neural crest cells within the hindbrain region of the chick. Dev. Dyn. 232, 939–949.
Perez-Alcala, S., et al., 2004. LSox5 regulates RhoB expression in the neural tube and promotes generation of the neural crest. Development 131, 4455–4465. Epub 2004 Aug 11.
Renaud, J., et al., 2008. Plexin-A2 and its ligand, Sema6A, control nucleus-centrosome coupling in migrating granule cells. Nat. Neurosci. 11, 440–449.
Ridley, A.J., et al., 2003. Cell migration: integrating signals from front to back. Science 302, 1704–1709.
Santiago, A., Erickson, C.A., 2002. Ephrin-B ligands play a dual role in the control of neural crest cell migration. Development 129, 3621–3632.
Sato, M., et al., 2006. Semaphorin3D regulates invasion of cardiac neural crest cells into the primary heart field. Dev. Biol. 298, 12–21. Epub 2006 Jun 2.
Serini, G., et al., 2003. Class 3 semaphorins control vascular morphogenesis by inhibiting integrin function. Nature 424, 391–397.
Song, H., et al., 1998. Conversion of neuronal growth cone responses from repulsion to attraction by cyclic nucleotides. Science 281, 1515–1518.
Stoller, J.Z., Epstein, J.A., 2005. Cardiac neural crest. Semin. Cell. Dev. Biol. 16, 704–715. Epub 2005 Jul 27.
Strachan, L.R., Condic, M.L., 2004. Cranial neural crest recycle surface integrins in a substratum-dependent manner to promote rapid motility. J. Cell Biol. 167, 545–554. Epub 2004 Nov 1.
Suda, T., Nagata, S., 1994. Purification and characterization of the Fas-ligand that induces apoptosis. J. Exp. Med. 179, 873–879.
Suto, F., et al., 2005. Plexin-a4 mediates axon-repulsive activities of both secreted and transmembrane semaphorins and plays roles in nerve fiber guidance. J. Neurosci. 25, 3628–3637.
Suto, F., et al., 2007. Interactions between Plexin-A2, Plexin-A4, and Semaphorin 6A Control Lamina-Restricted Projection of Hippocampal Mossy Fibers. Neuron 53, 535–547.
Takahashi, T., et al., 1998. Semaphorins A and E act as antagonists of neuropilin-1 and agonists of neuropilin-2 receptors. Nat. Neurosci. 1, 487–493.
Tamagnone, L., et al., 1999. Plexins are a large family of receptors for transmembrane, secreted, and GPI-anchored semaphorins in vertebrates. Cell 99, 71–80.
Torres-Vazquez, J., et al., 2004. Semaphorin-plexin signaling guides patterning of the developing vasculature. Dev. Cell. 7, 117–123.
Toyofuku, T., et al., 2007. Semaphorin-4A, an activator for T-cell-mediated immunity, suppresses angiogenesis via Plexin-D1. EMBO J. 26, 1373–1384. Epub 2007 Feb 22.
Toyofuku, T., et al., 2005. FARP2 triggers signals for Sema3A-mediated axonal repulsion. Nat. Neurosci. 8, 1712–1719. Epub 2005 Nov 13.
Toyofuku, T., et al., 2004a. Dual roles of Sema6D in cardiac morphogenesis through region-specific association of its receptor, Plexin-A1, with off-track and vascular endothelial growth factor receptor type 2. Genes Dev. 18, 435–447. Epub 2004 Feb 20.
Toyofuku, T., et al., 2004b. Guidance of myocardial patterning in cardiac development by Sema6D reverse signalling. Nat. Cell. Biol. 6, 1204–1211. Epub.
Vielmetter, J., et al., 1990. In vitro assay to test differential substrate affinities of growing axons and migratory cells. Exp. Brain Res. 81, 283–287.
Waldo, K., et al., 1998. Cardiac neural crest cells provide new insight into septation of the cardiac outflow tract: aortic sac to ventricular septal closure. Dev. Biol. 196, 129–144.
Wang, H.U., Anderson, D.J., 1997. Eph family transmembrane ligands can mediate repulsive guidance of trunk neural crest migration and motor axon outgrowth. Neuron 18, 383–396.
Winberg, M.L., et al., 1998. Plexin A is a neuronal semaphorin receptor that controls axon guidance. Cell 95, 903–916.
Wu, W., et al., 1999. Directional guidance of neuronal migration in the olfactory system by the protein Slit. Nature 400, 331–336.
Yu, H.H., et al., 2000. Semaphorin-1a acts in concert with the cell adhesion molecules fasciclin II and connectin to regulate axon fasciculation in Drosophila. Genetics 156, 723–731.

Tumor angiogenesis and progression are enhanced by Sema4D produced by tumor-associated macrophages

Jose Rafael Sierra,[1] Simona Corso,[1] Luisa Caione,[1] Virna Cepero,[1] Paolo Conrotto,[1] Alessandro Cignetti,[1] Wanda Piacibello,[1] Atsushi Kumanogoh,[2] Hitoshi Kikutani,[2] Paolo Maria Comoglio,[1] Luca Tamagnone,[1] and Silvia Giordano[1]

[1]Institute for Cancer Research and Treatment, University of Torino Medical School, 10060 Candiolo (Torino), Italy
[2]Research Institute for Microbial Diseases, Osaka University, Osaka 565-0871, Japan

Increased evidence suggests that cancer-associated inflammation supports tumor growth and progression. We have previously shown that semaphorin 4D (Sema4D), a ligand produced by different cell types, is a proangiogenic molecule that acts by binding to its receptor, plexin B1, expressed on endothelial cells (Conrotto, P., D. Valdembri, S. Corso, G. Serini, L. Tamagnone, P.M. Comoglio, F. Bussolino, and S. Giordano. 2005. *Blood.* 105:4321–4329). The present work highlights the role of Sema4D produced by the tumor microenvironment on neoplastic angiogenesis. We show that in an environment lacking Sema4D, the ability of cancer cells to generate tumor masses and metastases is severely impaired. This condition can be explained by a defective vascularization inside the tumor. We demonstrate that tumor-associated macrophages (TAMs) are the main cells producing Sema4D within the tumor stroma and that their ability to produce Sema4D is critical for tumor angiogenesis and vessel maturation. This study helps to explain the protumoral role of inflammatory cells of the tumor stroma and leads to the identification of an angiogenic molecule that might be a novel therapeutic target.

CORRESPONDENCE
Silvia Giordano:
silvia.giordano@unito.it

Abbreviations used: b-FGF, basic fibroblast growth factor; EC, endothelial cell; HGF, hepatocyte growth factor; HUVEC, human umbilical vein endothelial cell; MSR1, macrophage scavenger receptor 1; Sema4D, semaphorin 4D; TAM, tumor-associated macrophage; VSV, vesicular stomatitis virus.

Semaphorins are a large family of either membrane-bound or secreted proteins that were originally described in the nervous system, where they are involved in the establishment of a correct neuronal network (1, 2). These ligands exert their activities by binding to high affinity receptors known as plexins, a family of transmembrane molecules that share structural homology with semaphorins themselves (3). An increasing amount of data show that these two protein families also exert their action outside the nervous system, as they play a critical role in cardiac and skeletal development (4, 5), immune response (6, 7), epithelial morphogenesis (8), and tumor growth and metastatization (9, 10). Moreover, studies suggest that these molecules are important players during angiogenesis, as they regulate blood vessel growth and endothelial cell (EC) homing during vessel development (11). Although secreted class III semaphorins inhibit EC migration and in vitro vessel formation (12), class IV semaphorins positively regulate angiogenesis (13, 14). Angiogenesis is a complex, multistep process in which ECs of preexisting blood vessels, challenged by appropriate biochemical and physical cues, dynamically remodel their cell-to-cell and cell-to-matrix adhesions and reorganize themselves into a mature, hierarchically organized system of hollow endothelial tubes that is eventually stabilized by interaction with pericytes.

We and others have identified semaphorin 4D (Sema4D), also known as CD100, as a potent proangiogenic molecule (13–17). Sema4D, originally discovered in the immune system, where it regulates B cell aggregation and survival and T cell activation (18, 19), can be found either as a 150-kD membrane-bound form or as a 120-kD soluble molecule; the latter is originated as a consequence of a proteolytic cleavage (17, 20, 21). Sema4D acts by binding to its high affinity receptor, plexin B1 (3), to an intermediate

P. Conrotto's present address is Dept. of Chemistry and Applied Biosciences, ETH Zurich, 8093 Zurich, Switzerland.
The online version of this article contains supplemental material.

J. Exp. Med. Vol. 205 No. 7 1673-1685 www.jem.org/cgi/doi/10.1084/jem.20072602

affinity receptor, plexin B2 (both of which are widely expressed) (22), or to a low affinity receptor, CD72, which is mainly expressed by cells of the hematopoietic lineage (23). Sema4D and plexin B1/B2 share structural homology with the tyrosine kinase receptors c-Met and Ron (24, 25). We have previously shown that activation of plexin B1 through Sema4D binding transactivates c-Met and promotes the invasive ability of tumor cells (8). Moreover, we have also demonstrated that Sema4D, upon binding plexin B1 and activating c-Met, promotes angiogenesis both in vitro and in vivo (13).

Reports have recently pointed out the close correlation between inflammatory infiltration of the tumor stroma and a high vascular grade (26, 27). Because Sema4D is produced by inflammatory cells present in the tumor microenvironment (7), we wanted to assess whether stroma-derived Sema4D could influence the tumorigenic ability of cells as well as their capacity to originate metastasis. In this paper, we show that in an environment lacking Sema4D, the ability of breast cancer cells to originate tumor masses and metastases is severely impaired. This impairment is paralleled by an altered vascularization inside the tumor. We also provide evidence that the main cells producing the semaphorin in the tumor stroma are the tumor-associated macrophages (TAMs), and that TAM-derived Sema4D is critical for tumor angiogenesis and for the maturation of blood vessels. This work thus highlights a novel function of cells involved in the inflammatory response of tumors and identifies Sema4D as a new player in the complex interaction between tumor cells and the tumor microenvironment.

RESULTS

Tumor growth and metastatic ability of breast cancer cells is impaired in Sema4D KO mice

Previous works have shown that Sema4D is endowed with angiogenic properties, both in vitro and in vivo (13–15). However, Sema4D is dispensable for the formation of vessels during embryogenesis, as Sema4D KO mice are viable (19). To investigate if Sema4D might play a role in pathological vasculogenesis, such as that taking place in tumors, we grafted syngeneic tumor cells (TSA, breast cancer) both in WT and in Sema4D KO (KO) mice. As shown in Fig. 1 A, tumor growth was significantly impaired in mice lacking Sema4D in comparison to WT mice (an almost sixfold reduction at the end of the experiment: $P < 0.0001$). Similar experiments performed with three other breast cancer cell lines (66cl4, 4T1, and 168FARN) gave similar results, as the grafted cells originated smaller tumors in KO mice in comparison to the WT animals (Fig. S1, available at http://www.jem.org/cgi/content/full/jem.20072602/DC1).

We have previously demonstrated that Sema4D acts not only on ECs but also on tumor cells and that it stimulates their invasive ability (8). After proving that TSA cells do express plexin B1, the high affinity receptor for Sema4D, and display enhanced in vitro motility and invasiveness in response to the semaphorin (Fig. S2, available at http://www.jem.org/cgi/content/full/jem.20072602/DC1), we evaluated their metastatic ability in KO and WT mice. As shown in Fig. 1 (B–D), we observed a reduced incidence of metastases in KO versus WT mice ($P < 0.0001$). Collectively, these results indicate that the presence of Sema4D in the tumor microenvironment contributes to tumor growth and metastasis.

Maturation of tumor vessels is impaired in Sema4D KO mice

We wondered if the decreased tumorigenic ability observed in Sema4D KO mice could be caused by altered vasculogenesis. Thus, we stained slices of tumors of comparable size, grown either in WT or KO mice, with anti-CD31 antibody (a marker of ECs; Fig. 2 A). Although the total number of vessels was similar in the two types of animals (Fig. 2 B, top), the total vessel area and mean vessel size were significantly smaller in tumors grown in Sema4D KO mice ($P < 0.0001$; Fig. 2 B, middle and bottom).

Interactions between ECs and pericytes in the vessel walls have been recently identified as central processes in the regulation of vascular formation, stabilization, remodeling, and function (28). Failure of the interactions between these cell types has been described in some human pathologies, including tumor angiogenesis (29). Because pericytes are recruited by stromal-derived cytokines (30), we decided to verify if they were normally localized along the altered vessels of tumors grown in Sema4D KO mice. We thus stained tumor slices with anti-NG2, an antibody that identifies pericytes. As shown in Fig. 2 C, vessels of tumors originated in KO mice very rarely showed a normal interaction between ECs and pericytes. Most of them, in fact, were negative for the presence of pericytes, which were instead normally present in tumors that originated in control mice. Collectively, these observations suggest that Sema4D plays a role in tumor angiogenesis, where it contributes to the maturation of tumor vessels by acting on ECs and favoring the recruitment of pericytes.

Bone marrow–derived cells produce Sema4D that contributes to tumor growth and vessel organization

The results of the previous experiments suggest that cells of the tumor microenvironment produce the Sema4D that is required to promote tumor angiogenesis. To identify these cells, we performed immunofluorescent stainings on tumor slices. As shown in Fig. 3 A, most of the cells positive for Sema4D were also stained by an anti-CD45 mAb, suggesting that they belong to the leukocyte lineage ($P < 0.0001$).

To prove that bone marrow–derived cells are indeed the major producers of the semaphorin, we performed bone marrow transplantation experiments. We injected WT male–derived bone marrow cells into female KO animals. PCR analyses performed 2 wk later (evaluating the presence of the Y chromosome in peripheral leukocytes) showed that the mice were chimeric, with ~70% of their leukocytes derived from WT marrow (Fig. 3 B, bottom). We thus injected these chimeric mice with tumor cells and evaluated tumor growth. As shown in Fig. 3 B, tumors grown in chimeric KO mice were bigger than those grown in KO animals. As expected, we found many $CD45^+$ cells expressing Sema4D in tumors grown in KO mice transplanted with WT bone marrow (unpublished data).

We also performed the reverse experiment by analyzing tumor growth in lethally irradiated (900 cGy) WT female mice transplanted with bone marrow cells derived from KO male mice (Fig. 3 C, bottom). As shown in Fig. 3 C, tumors grown in WT mice transplanted with KO-derived bone marrow cells were smaller compared with those grown in WT animals transplanted with WT bone marrow. When we counted $CD45^+$ cells inside tumors, we observed a slight decrease of bone marrow–derived cells in mice transplanted with KO bone marrow versus those transplanted with WT bone marrow (mean $CD45^+$ cells/field = 48.5 ± 8.7 and 38.7 ± 7.8, respectively). When we analyzed tumor vascularization, we found a high vascular grade only in tumors grown in mice having WT bone marrows (either endogenous or transplanted; Fig. 3, D and E). Collectively, these experiments suggest that in the tumor microenvironment, bone marrow–derived cells produce the Sema4D that contributes to vessel maturation and, eventually, tumor growth.

Sema4D produced by platelets does not contribute to tumor growth

It has been recently reported that activated platelets express Sema4D and that the surface expression of the semaphorin increases during platelet activation, followed by the gradual

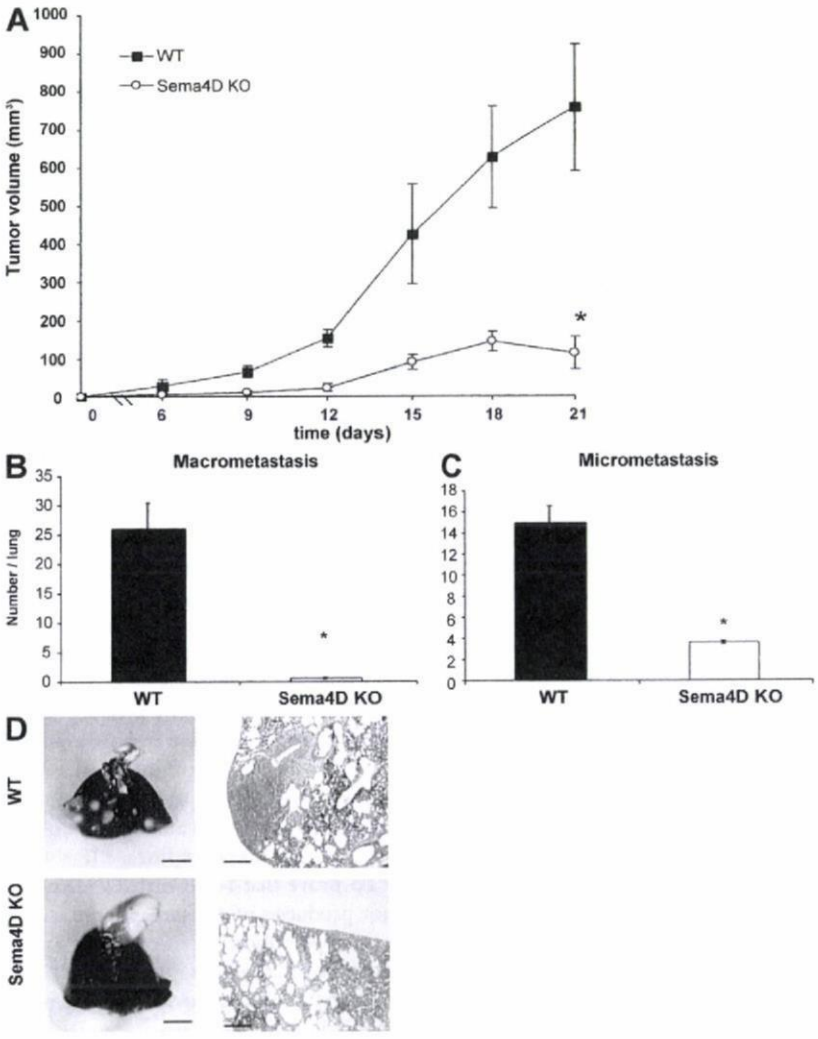

Figure 1. Tumor growth and metastatic ability of breast cancer cells is impaired in Sema4D KO mice. (A) TSA breast cancer cells were subcutaneously injected in WT and Sema4D KO mice. Tumor volume was evaluated at the indicated days. As shown, tumor burden was dramatically less in Sema4D KO versus WT mice. Bars indicate mean tumor volume ± SEM. *, $P < 0.0001$ ($n = 10$ mice per group). (B and C) Macro- and micrometastases present in the lungs of mice bearing tumors of comparable size were evaluated as indicated in Materials and methods and scored. Error bars indicate mean ± SD. *, $P < 0.0001$ ($n = 10$ lungs). (D) Representative pictures of lungs and lung slices for WT and Sema4D KO mice. As shown, the number of metastases was significantly lower in Sema4D KO mice. Statistical differences between groups were determined by using the two-tailed Student's *t* test. Bars: (whole mount) 0.5 cm; (micrograph) 0.2 mm.

shedding of its extracellular domain (21). It is widely accepted that blood clotting can contribute to tumor growth and dissemination by creating a fibrin clot surrounding tumor cells that can protect them from apoptosis (31). We wondered if platelets could be the bone marrow–derived elements contributing the Sema4D responsible for tumor promotion. We thus grafted TSA cells in WT and in KO mice chronically treated with clopidogrel, a widely used inhibitor of platelet activation (32). Platelet inactivation was proven by analyzing the expression of CD62P on platelets obtained from

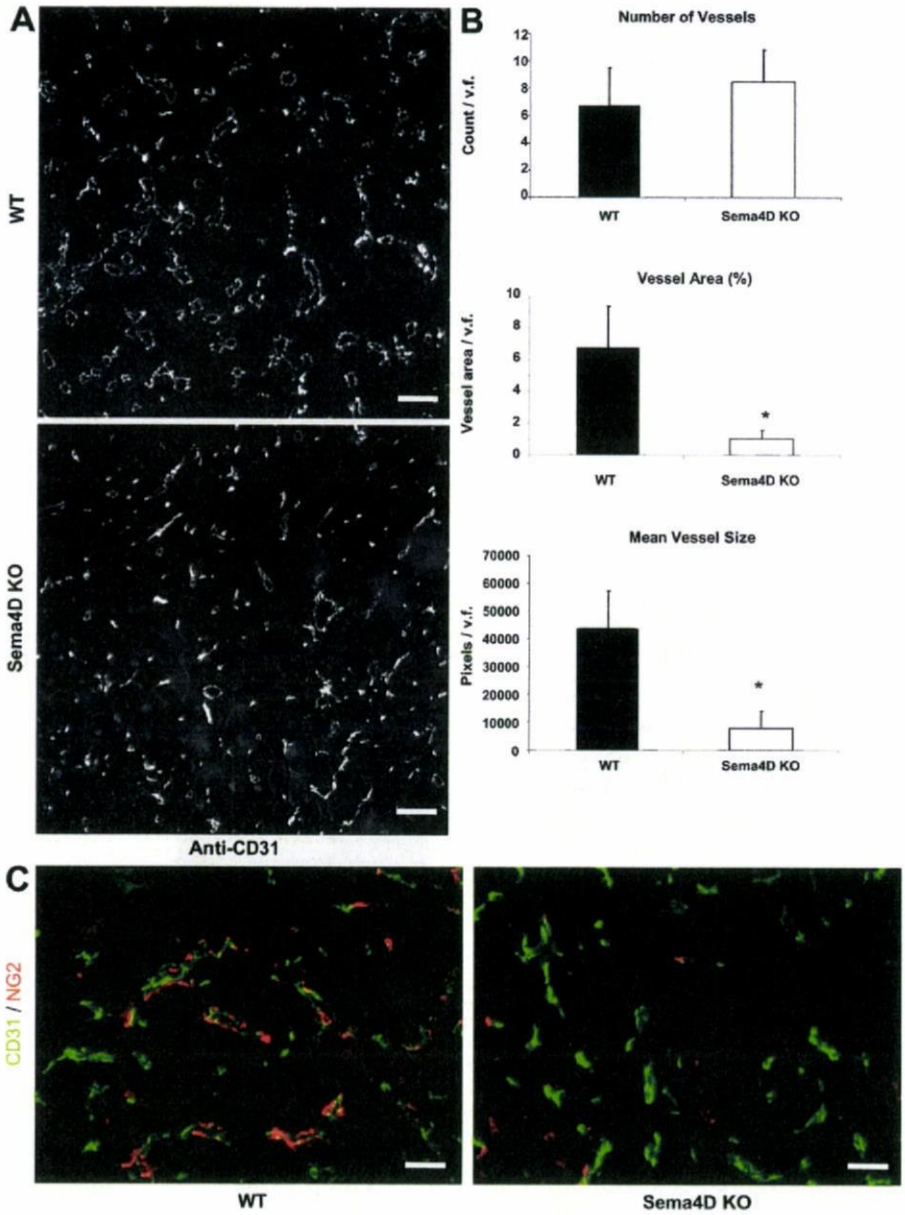

Figure 2. Tumor vascularization is altered in Sema4D KO mice. (A and B) Evaluation of tumor vascularization. Blood vessel staining of tumor histological sections was performed with an anti-CD31 antibody. The number and area of vessels were evaluated by fluorescence microscopy. As shown, although the number of vessels is not significantly different, vessel area and size are significantly reduced in Sema4D KO mice. Error bars indicate mean ± SD. *, $P < 0.0001$ ($n = 8$ mice per group, with 10 fields per animal). Bars, 100 µm. (C) To evaluate the presence of vessel-associated pericytes, tumor sections were costained with the pericyte-specific antibodies NG2 (red) and CD31 (green). Analysis was performed on one slice per mouse ($n = 8$ mice per group). As shown, vessels of tumors that originated in KO mice very rarely showed a normal interaction between ECs and pericytes, and in most cases they stained negative for the presence of pericytes (right), which were instead normally present in tumors originated in control mice (left). Statistical differences between groups were determined by using the two-tailed Student's *t* test. v.f., visual field. Bars, 50 µm.

treated and untreated animals. Mice treated with clopidogrel failed to expose CD62P on their membrane (unpublished data). As shown in Fig. S3 (available at http://www.jem.org/cgi/content/full/jem.20072602/DC1), we did not observe significant changes in the growth of tumor xenografts in mice in which platelet activation was inhibited. Similar results were obtained when platelet activation was inhibited by aspirin (unpublished data). These experiments indicate that platelet-derived Sema4D is not critical to elicit the tumorigenic ability of breast cancer cells.

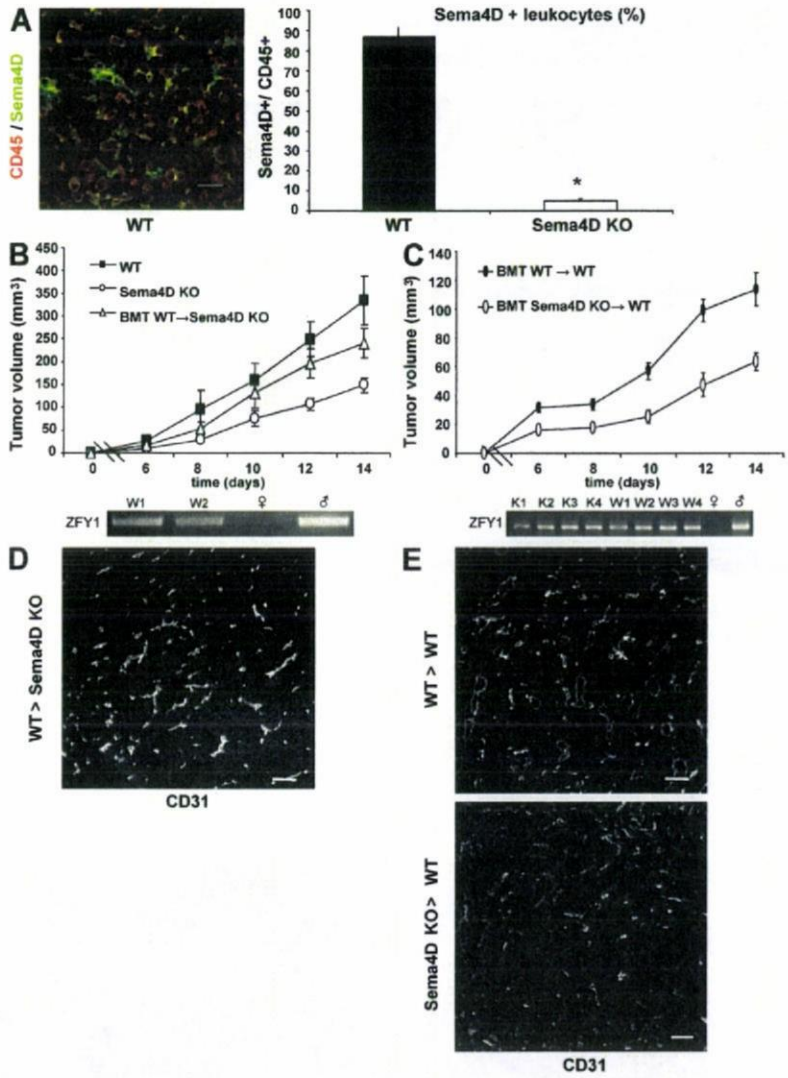

Figure 3. Bone marrow–derived cells produce Sema4D that contributes to tumor growth and vessel organization. (A) CD45⁺ cells express Sema4D. To evaluate whether CD45⁺ cells express Sema4D, tumor slices were costained with CD45 and Sema4D antibodies. Double-positive cells were then counted on 10 slices per group (one slice per tumor). (right) As shown, ~85% of the leukocytes express Sema4D. Error bars indicate mean ± SD. *, $P < 0.0001$. Bar, 50 µm. (B) WT-derived bone marrow cells rescue tumor burden. (top) The mean volume ± SEM of grafted tumors in WT mice, Sema4D KO mice, and Sema4D KO mice transplanted with WT-derived bone marrow (BMT; $n = 6$ tumors per group). As shown, tumors grown in transplanted KO mice were bigger than those grown in nontransplanted KO mice. (bottom) PCR amplification of the ZFY1 gene on the Y chromosome from DNA derived from peripheral leukocytes. As shown, transplanted mice were chimeric, displaying ~70% of leukocytes derived from the donors (for experimental details, see Materials and methods). W1 and W2 indicate representative transplanted mice, and female and male DNA are shown. (C) Sema4D KO bone marrow transplantation leads to decreased tumor burden in WT females. Lethally irradiated (900 cGy) WT females were transplanted with bone marrow cells derived from KO or WT male mice ($n = 8$ tumors per group). Bars indicate mean volume ± SEM. As in B, engraftment was confirmed by PCR analysis (bottom). K, Sema4D KO mice. (D and E) Tumor vessels resemble the phenotype of the original bone marrow donor when stained by CD31 antibody (compare with Fig. 2). D shows vessels, stained with CD31 antibodies, in a tumor grown in Sema4D KO mice transplanted with WT bone marrow. E shows slices derived from tumors grown in WT animals transplanted with WT (top) or KO (bottom) bone marrow. Statistical differences between groups were determined by using the two-tailed Student's *t* test. Bars, 100 µm.

Macrophages are the main source of Sema4D in the tumor microenvironment

As shown in Fig. 3 B, we have observed that transplantation of bone marrow from WT to KO animals could rescue the impairment of tumor growth. In recent years, compelling evidence supports the idea that TAMs, which account for the majority of the infiltrating inflammatory cells into the tumor mass and exhibit a phenotype distinct from any other activated monocytes, play an integral role during tumor progression (33). These cells, in fact, produce cytokines that aid the proliferation and survival of tumor cells, as well as their ability to invade surrounding tissues and metastasize (34–36). Immunofluorescence revealed that most of the leukocytes in the tumor stroma were indeed macrophages (Fig. 4 A), and that they expressed Sema4D (Fig. 4, B and C).

To evaluate if the expression of Sema4D is linked to monocyte/macrophage differentiation or to macrophage activation, we performed some in vivo experiments. We induced experimental peritonitis in mice by injection of CFA; 3 d later, we collected peritoneal macrophages and compared the expression of Sema4D on these cells versus resident peritoneal macrophages obtained from control mice. As shown

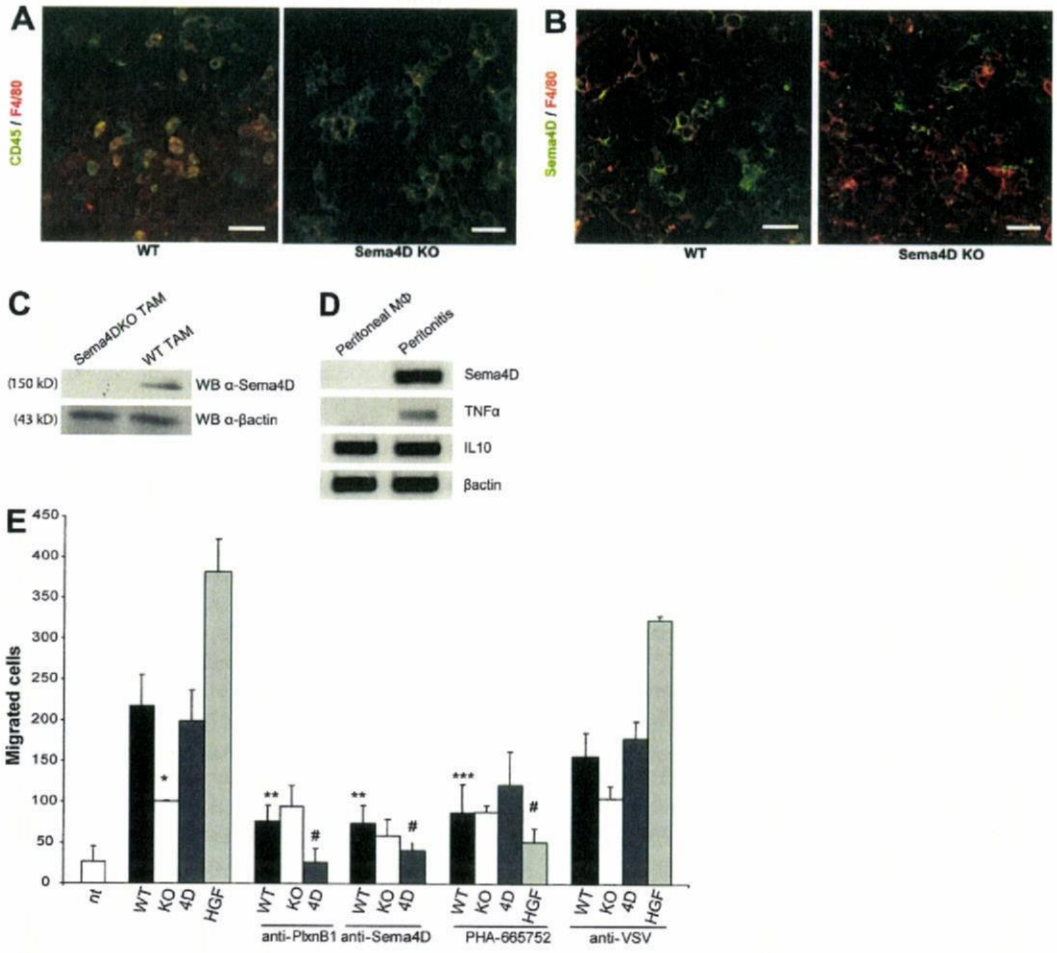

Figure 4. TAMs produce Sema4D that acts on ECs. (A and B) Immunofluorescence analysis of tumors grown in WT or Sema4D KO animals. In A, staining with CD45 and F4/80 (specific for macrophages) reveals that most of the leukocytes in the tumor stroma are macrophages (~90%; not depicted). In B, staining with F4/80 and Sema4D antibody reveals that TAMs express Sema4D. Bars, 50 µm. (C) Western blot analysis of total cell lysates of TAMs derived from WT or Sema4D KO mice. The blot was probed with anti-Sema4D antibodies and, as a loading control, with anti-β-actin. (D) PCR analysis performed on RNAs obtained from peritoneal macrophages of control mice (left) or of mice injected i.p. with CFA. As shown, only activated macrophage express Sema4D. (E) Transwell motility assays. The ability of supernatants of cultures of TAMs, purified from tumors grown either in WT or KO mice, to promote EC (HUVEC) migration was evaluated. Supernatants of WT TAMs efficiently promoted EC migration, whereas supernatants of KO TAMs were significantly less effective. Moreover, the chemoattractive activity of the WT supernatant was significantly decreased in the presence of Sema4D or plexin B1 blocking antibodies, and of the c-Met inhibitor PHA-665752. Chemoattractive positive controls included Sema4D (4D) and HGF, whereas anti-VSV was used as a control antibody. Bars represent the mean ± SD (experiments were performed twice in triplicate). Statistical differences between groups were determined by using the two-tailed Student's *t* test. *, P = 0.0003; **, P = 0.0002; ***, P = 0.0013; and #, P = 0.0001.

in Fig. 4 D, although Sema4D was not expressed in resting macrophages, it was up-regulated in activated macrophages. Similar results were also obtained from the analysis of human cells; in fact, although monocytes did not express Sema4D, activated macrophages did (Fig. S4, available at http://www.jem.org/cgi/content/full/jem.20072602/DC1). Moreover, we found that, in vitro, Sema4D expression was not induced by differentiating stimuli (M-CSF, PMA, IL-10, or TGF-β), whereas it was induced by activating molecules (such as LPS; Fig. S4). All of these data suggest that the expression of Sema4D is not strictly liked to monocyte/macrophage differentiation, and that this molecule is expressed on different types of activated macrophages.

We then analyzed whether macrophages of KO mice behaved normally in term of response to activating stimuli and of cytokine production. As shown in Fig. S5 (available at http://www.jem.org/cgi/content/full/jem.20072602/DC1), macrophages from Sema4D KO mice were indeed able to respond to LPS by increasing the production of cytokines such as TNF-α. Moreover, we did not observe significant differences in cytokine production between WT- and KO-derived TAMs (Fig. S5), or in their ability to differentiate in M2 TAMs (as shown by the expression of macrophage scavenger receptor 1 [MSR1], a marker of this cell type). However, we observed that the mean number of macrophages recruited to the tumor was lower in Sema4D KO than in WT mice (19.03 ± 5.2 and 35.57 ± 4.2 F4/80$^+$ cells/field, respectively).

To prove the role of TAM-produced Sema4D in tumor angiogenesis and growth, we performed several experiments. To begin, we purified and cultured TAMs from tumors grown both in WT and KO mice (37). Although the supernatant of cultures of WT TAMs was able to efficiently promote EC migration, the supernatant of KO TAMs was significantly less effective; moreover, the chemoattractive activity of WT supernatant was partially lost in the presence of Sema4D or plexin B1 blocking antibodies (Fig. 4 E) (16, 38).

Because we have previously shown that recruitment of the c-Met tyrosine kinase receptor by the activated Sema4D receptor (plexin B1) is required for the angiogenic ability of Sema4D, we wondered if c-Met inhibition impaired TAM-induced EC motility. In line with our previous results, inhibition of c-Met with the small molecule PHA-665752 (39) resulted in a significant decrease of EC motility in response to WT TAM supernatant (Fig. 4 E).

To evaluate the in vivo angiogenic role of TAMs, Matrigel plugs containing either WT or KO TAMs were subcutaneously implanted in KO mice. After 14 d, mice received dextran-FITC and were killed. As shown in Fig. 5 A, Matrigel plugs containing known angiogenic factors (such as hepatocyte growth factor [HGF] or basic fibroblast growth factor [b-FGF]) displayed several well-organized vessels, plugs containing WT TAMs were also well vascularized and showed well-formed and branched vessels, and plugs containing KO TAMs displayed small and poorly organized vessels. Addition of blocking plexin B1 antibodies (ec6.9), as well as of the c-Met inhibitor PHA-665752, resulted in the lack of an organized vessel tree, suggesting that activation of these two receptors is mandatory for the Sema4D-induced angiogenic response.

Sema4D produced by TAMs increases the tumorigenic ability of cancer cells

To finally prove that the ability of TAMs to produce Sema4D contributes to the tumorigenic ability of cancer cells, we coinjected TSA tumor cells and TAMs obtained either from WT or KO animals in KO mice. Coinjection of TSA cells and WT TAMs resulted in the formation of significantly larger tumor masses in comparison to those originated by TSA plus KO TAMs (Fig. 5 B). We found a comparable number of TAMs (F4/80$^+$ cells) in the tumors of both groups of animals; moreover, we could detect positivity for Sema4D only in KO mice injected with WT TAMs (unpublished data). As expected, in the presence of WT or KO TAMs, tumor growth was enhanced in comparison to tumor cells alone, in agreement with the previously described protumorigenic role of these cells (35).

DISCUSSION

Tumor development is a complex event that involves not only tumor cells but also the surrounding stroma. In recent years, in fact, data collected both from experimental systems and clinical observations have strengthened the idea that the tumor microenvironment and neoplastic cells act in concert and contribute as a functional whole to the growth and progression of the tumor mass (33). This idea was originally proposed by Paget's famous "seed and soil" hypothesis, which highlighted the possible contribution of stromal cells to the process of tumorigenesis (33).

The mechanisms promoting tumor angiogenesis are not yet fully understood, but it is believed that the most important factor is tumor hypoxia, which induces the release of angiogenic molecules from tumor cells, attracting ECs and inflammatory cells. Recruited ECs migrate toward the hypoxic areas, whereas inflammatory cells, in turn, secrete molecules that intensify the angiogenic stimulus. Once ECs are engaged, perivascular support cells stabilize nascent vessels and guarantee appropriate blood flow (28). Many molecules involved in these processes have been identified, and it has recently become clear that most of them originate from stromal cells recruited to the tumor microenvironment (30). Tumor-infiltrating inflammatory cells undergo a process of maturation or "education" within the tumor microenvironment (40), and pharmacological or genetic inhibition of molecules that are up-regulated in these cells was indeed shown to be able to impair tumor progression in animal models (33).

In this scenario, a critical role has been demonstrated for TAMs that represent the major inflammatory component of the stroma of many tumors (41). Experimental models have demonstrated that the lack of recruitment of macrophages at the tumor site results in decreased tumorigenic ability (42), and clinical evidence has shown that there is a correlation between a high TAM content inside the tumor and a poor prognosis (41). These results have been recently confirmed

by gene profiling data showing that genes associated to leukocyte or macrophage infiltration are part of the molecular signatures linked to a poor prognosis in breast cancer (43). In this line, the identification of macrophage-derived molecules that support the protumoral activity of these cells becomes very important.

Sema4D is a proangiogenic factor (13–17), but this activity is dispensable for "normal" angiogenesis because Sema4D KO mice are viable (19). It has been previously shown that tumor angiogenesis is partially different from the norm (in fact, tumor vessels are often abnormal in structure and function) and is characterized by an altered vessel maturation, possibly because of an inappropriate balance between vasculogenic and angiogenic factors (44). We thus wondered if Sema4D could play any role in tumor angiogenesis. In this paper, we show that Sema4D is required for proper vessel maturation in tumors, as its deficiency results in the presence of vessels of smaller diameter that are poorly lined by perimural cells, such

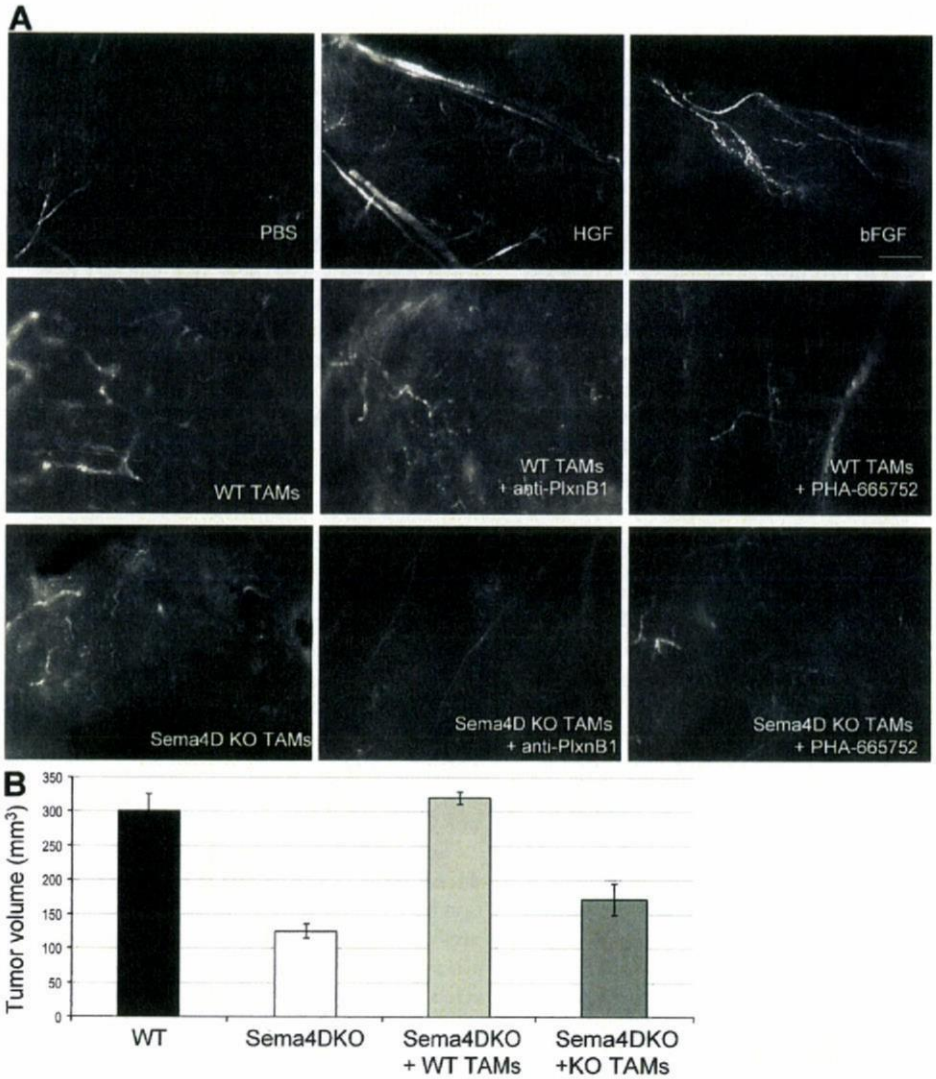

Figure 5. Sema4D produced by TAMs promotes angiogenesis and increases the tumorigenic ability of cancer cells. (A) Matrigel plugs containing either WT or KO TAMs were subcutaneously implanted in KO mice. After 14 d, mice received dextran-FITC and were killed, and plugs were microscopically analyzed. As shown, plugs containing WT TAMs were well vascularized and showed well-formed and branched vessels, whereas plugs containing KO TAMs displayed small and poorly organized vessels. Addition of blocking plexin B1 antibodies, as well as of the c-Met inhibitor PHA-665752, resulted in the lack of an organized vessel tree. Plugs containing PBS were used as a negative control, whereas plugs containing known angiogenic factors (HGF and b-FGF) were used as positive controls. ($n = 3$ plugs per group). Bar, 2 mm. (B) TSA tumor cells were injected in KO mice alone or together with TAMs obtained either from WT or KO animals. TSA cells alone were also injected in WT mice as a control. Coinjection of TSA cells and WT TAMs resulted in the formation of significantly larger tumor masses in comparison to those originated by TSA plus KO TAMs. Bars represent the mean ± SEM.

as pericytes. Interestingly, we have observed that the number of lymphatic vessels in the tumors is not altered in Sema4D KO mice (unpublished data). We also demonstrate that the angiogenic Sema4D is produced by stromal cells infiltrating the tumor. Although another paper has shown an angiogenic role of tumor-derived Sema4D (16), we could not observe a different behavior of breast cancer cells, either producing Sema4D (TSA, 4T1, and 168FARN; unpublished data) or not (66cl4; reference 45), when they where subcutaneously injected in KO mice. Moreover, when we silenced the expression of this semaphorin in the producing cells, we did not observe any significant difference compared with control cells (Fig. S6, available at http://www.jem.org/cgi/content/full/jem.20072602/DC1). A possible reason for these divergences can be caused by the different tumor types used in the two experimental systems. In breast cancer, in fact, a very good correlation has been established between the presence of a strong inflammatory component, mainly containing TAMs, and the malignant behavior (35, 43). It is possible that the head and neck carcinoma cells used by Basile et al. (16) rely on different mechanisms to promote angiogenesis and are less dependent on the tumor microenvironment.

The tumor stroma contains several cell types, either "resident" (such as fibroblasts or adipocytes) or "infiltrated." Because most of the Sema4D$^+$ cells were also positive for leukocyte markers, we hypothesized that they were blood-derived cells. Bone marrow transplantation experiments formally proved that the Sema4D-producing cells are indeed of hematopoietic origin, as we could recover the WT phenotype (concerning tumor growth and angiogenesis) by transplanting a WT bone marrow into Sema4D KO mice.

A recent report has highlighted the role of Sema4D in platelet activation and thrombus formation (21). Because it is known that blood clotting contributes to tumor growth and dissemination by creating a fibrin clot surrounding tumor cells that can protect them from apoptosis (31), we investigated whether platelet-derived Sema4D could contribute to tumor growth. Chronic treatment of mice with clopidogrel and aspirin did not result in significant changes in the growth of grafted tumors either in WT or KO mice. These results suggest that platelet-derived Sema4D is not required for tumor angiogenesis.

Among the cells of the tumor stroma, we found the highest levels of Sema4D in TAMs, expressing markers of the M2 type. These cells are known to tune inflammatory responses and adaptive Th2 immunity, to scavenge debris, and to promote angiogenesis, tissue remodeling, and repair (35). We found that M2-type TAMs were also present in the microenvironment of Sema4D KO mice and that the absence of this molecule did not significantly affect their functional response to activating stimuli and their ability to produce cytokines. However, the inability of TAMs to produce Sema4D strongly decreased their capacity to attract ECs, in vitro and in vivo, and to promote vessel maturation. Moreover, WT-derived TAMs coinjected with tumor cells in KO animals were able to promote tumor growth at similar levels as in WT mice.

We show that Sema4D exerts its activity on ECs through its high affinity receptor plexin B1, as demonstrated by the lack of chemotactic and angiogenic responses in the presence of plexin B1 blocking antibodies. Moreover, as previously reported (8, 13), plexin-induced c-Met activation is a crucial event in Sema4D signal transduction, as c-Met inhibition resulted in the loss of Sema4D-induced biological responses.

On the basis of the reported results and of data derived from the literature, how can we figure the activity of Sema4D in the tumor stroma? We propose the following model. Cancer cells start to grow and reach a mass that becomes hypoxic. Hypoxia induces several changes in cancer cells and is a strong recruiting factor for TAMs. TAMs, indeed, accumulate preferentially in poorly vascularized tumor regions, where they stop and "adapt" to hypoxia by increasing the expression of hypoxia-inducible and proangiogenic genes (46, 47). Most of these activities are mediated by the hypoxia-responsive transcription of hypoxia-inducible factor 1; its inhibition, in fact, resulted in in vivo impairment of macrophage motility and activation (48). Among the genes induced by hypoxia are the *c-Met* tyrosine kinase (49) and *Sema4D* (17). TAM-derived Sema4D can thus trigger the plexin expressed by macrophages and activate c-Met. This receptor, in turn, promotes the production of several cytokines that can contribute to the protumorigenic activity of these cells (50). Among the several proteases produced by TAMs is membrane type 1 metalloproteinase (whose expression is also induced by hypoxia) (51), which can cleave the membrane-bound Sema4D and induce its release as a soluble protein (17) able to act on distant cells. Production of the soluble form has been shown to be critical for the angiogenic activity of Sema4D (17), as it can diffuse and act on ECs, stimulating angiogenesis, and on mural cells, promoting their recruitment. Secreted Sema4D can also stimulate the invasive ability of cancer cells (which very frequently express its receptor). In previous works, we have shown that this biological activity requires the recruitment of c-Met, probably facilitated by hypoxia-induced c-Met overexpression (8, 13, 49). Loss of c-Met activation can be one of the mechanisms contributing to the decreased metastatic ability of cancer cells grown in KO mice.

In conclusion, we have identified a novel molecule produced in the tumor stroma that can contribute to the interaction between the tumor microenvironment and tumor cells by promoting tumor angiogenesis and invasion. This molecule is produced by macrophages, a cell type that is strongly implicated in tumor progression and associated with a poor prognosis of several tumor types. As many attempts are now ongoing to target the tumor stroma, we propose Sema4D as a new candidate for antiangiogenic and antimetastatic cancer therapy.

MATERIALS AND METHODS

Cell culture

TSA, 66cl4, 168FARN, MLP29, and 4T1 cells were cultured in DMEM and were supplemented with 10% FBS, 100 U/ml penicillin, and 100 μg/ml streptomycin. Human umbilical vein endothelial cells (HUVECs) were cultured on 1% gelatin–coated dishes in endothelial cell basal medium-2 (Lonza) and were used at early passages (I–V).

In vivo tumorigenesis assay

All animal procedures were approved by the Ethical Commission of the University of Turin and by the Italian Ministry of Health. 5–8-wk-old Sema4D-deficient (19) and WT BALB/c mice (Charles River Laboratories) were injected with 5×10^5 TSA, 66cl4, or 168FARN cells and 10×10^4 4T1 cells subcutaneously in both posterior flanks. Tumor appearance was evaluated every 2 d using a caliper. Tumor volume was calculated using the formula $V = 4/3\pi \times (d/2)^2 \times (D/2)$, where d is the minor tumor axis and D is the major tumor axis.

Platelet inactivation. Clopidogrel treatment was administrated in the drinking water at a concentration of 0.26 mg/ml (equivalent to an oral dosage of ~30 mg/kg/day) (32). Aspirin was administered in the drinking water at a concentration of 0.3 mg/ml (equivalent to an oral dosage of ~30 mg/kg/day). Evaluation of platelet inactivation was performed by checking negativity of CD62p (BD Biosciences) by FACS.

Coinjection of TAMs. 2×10^5 TSA cells and 10^5 TAMs, WT or KO derived, were coinjected subcutaneously in the posterior flanks of Sema4D KO mice.

Lung metastases analyses. When tumors reached a volume of ~800 mm^3, animals were killed. We did not kill all of the mice at the same time; we allowed some tumors of KO mice to grow longer, to reach a size comparable with that observed in WT mice when they were killed. Lungs were contrasted with black India ink to facilitate scoring of superficial macrometastases. The analysis of micrometastases was performed on paraffin-embedded sections stained with hematoxylin and eosin.

Vessel counting. 10 random fields of eight representative tumor sections stained with anti-CD31 antibodies were analyzed as follows: vessels were counted manually using digital images taken with a microscope (DM IRB; Leica) connected to a camera (DC350FX; Leica) and analyzed with Metamorph 6.3 software (MDS Analytical Technologies). Vessel area is the total area occupied by vessels, whereas mean vessel size is vessel area/vessel number (as determined by averaging pixels contained inside of each vessel divided by the mean number of vessels). Structures without lumen at the magnification show in the figures were examined at higher magnification, and only structures with a lumen at higher enlargement were counted.

Analysis of in vivo–activated macrophages

On day 0, WT mice received a single i.p. injection of 0.1 ml CFA (Sigma-Aldrich) or 0.1 ml PBS. 3 d later, mice were killed. Peritoneal cells from control or treated mice were harvested by washing the peritoneal cavity with RPMI 1640 medium with 10% FBS. Cells were centrifuged at 1,200 rpm and washed twice with PBS. Cells were resuspended in RPMI 1640 serum-free medium and left to adhere for 1 h; nonadherent cells were removed by washing with PBS. Total RNA was extracted using a TRIZOL extraction kit (Invitrogen). 1 µg RNA was retrotranscribed using M-MLV reverse transcriptase minus H (Promega) in a final volume of 40 µl, according to the manufacturer's protocol. cDNA was later amplified by PCR using primers specific for each mouse cytokine.

Immunofluorescence

Immunofluorescent analyses were performed according to standard techniques. In brief, tumors were embedded on optimum cutting temperature–cryostat embedding compound. 4-µm sections were air dried and fixed in cold acetone. Sections were blocked for 2 h with blocking solution (2% goat serum, 1% BSA, 0.1% cold fish skin gelatin, 0.1% Triton X-100, 0.05% Tween 20, and 0.1 M PBS, pH 7.2). Primary antibodies were diluted 1:200 in antibody dilution solution containing 1% BSA, 0.1% cold fish skin gelatin, and 0.1 M PBS, pH 7.2, for 1 h. Anti-CD31, anti-CD45, and anti-Sema4D were purchased from BD Biosciences. Anti-F4/80 was purchased from AbD Serotec. Anti-NG2 was purchased from Chemicon. Sections were washed with TBS–0.1% Tween 20 and incubated for 30 min with secondary conjugated antibodies diluted 1:300 in TBS–0.1% Tween 20. Secondary antibodies were purchased from Invitrogen. Pictures were taken with a DM IRB microscope connected to a DC350FX camera and analyzed with Metamorph 6.3 software.

Transwell assay

5×10^4 TSA, 66cl4, and 4T1 cells or 3×10^4 HUVECs were seeded on the upper surface of 8-µm porous Transwell filters (Corning), coated on both sides with 3,000 ng/ml fibronectin. Upper chambers were filled with RPMI 1640 with 2% FBS, whereas lower chambers were supplied with RPMI 1640 with 2% FBS plus 6 nM Sema4D or 4 nM HGF (R&D Systems). For EC migration, RPMI 1640 with 2% FBS was placed in upper chambers, whereas TAM supernatants (WT or Sema4D KO) were placed in the lower chamber. Inhibitory molecules were added into the lower chamber compartment as follows: 100 ng/ml anti–plexin B1 (EC6.9; reference 52), 100 ng/ml anti-Sema4D (clone BMA-12; reference 19), 100 ng/ml anti–vesicular stomatitis virus (VSV; Sigma-Aldrich), and 100 nM PHA-665752 (Tocris Bioscience). As positive controls 6 nM Sema4D or 4 nM HGF (R&D Systems) were used. After 12 h of incubation, cells on the upper surface of the membrane were mechanically removed; cells that migrated to the lower face were fixed in 11% glutaraldehyde for 10 min and then stained with crystal violet for 5 min. Stained cells were quantified by counting.

Bone marrow transplantation

In one set of experiments, two tail-vein injections (with an interval of 1 h) of 8×10^7 male WT bone marrow cells were delivered into female Sema4D KO mice. In another set, lethally irradiated (900 cGy) female WT mice were injected with 5×10^6 male Sema4D KO or WT bone marrow cells. 2 wk after transplantation, genomic DNA was extracted (QIAGEN) from peripheral blood monocytes obtained from tail vein puncture. Genomic DNA was quantified and PCR amplified with ZFY1- and β-actin–specific primers: ZFY1 forward, 5′-CAATCCCCAAACCTGCTTGT-3′; ZFY1 reverse, 5′-CTCCCCTTCAGCTCTTCCTT-3′; b-act forward, 5′-GCTTACACTGCGCTTCTTGC-3′; and b-act reverse, 5′-AGAAAGGGCCACAGGAAGTC-3′. As a positive control, we used genomic DNA obtained from males; as a negative control, we used genomic DNA obtained from females. To quantify the engraftment, we compared the PCR products obtained from the genomic DNA of peripheral leukocytes of transplanted mice with the products of PCR reactions performed on a standard titration curve of a DNA mix containing different ratios of male/female genomic DNA.

TAM purification

TAM purification was performed as previously described (37). In brief, tumors grown in either WT or Sema4D KO mice were surgically removed, minced, and left to disaggregate in 0.125% trypsin in PBS with constant stirring at 37°C for 45 min. Trypsin was inactivated with FBS. Cells were later centrifuged and washed at 1,500 and 1,000 rpm with PBS. Cells were later left to adhere in serum-free RMPI 1640 for 1 h. Nonadherent cells were washed away. The remaining adherent cells were 90–95% $F4/80^+$. For supernatant collection, cells remained in serum-free conditions for 16 h and media were later collected.

Functional screening of peritoneal macrophages and TAMs

Peritoneal macrophages from WT or Sema4D KO mice were isolated and plated in DMEM containing 10% FBS. After 1 h of adherence, cells were washed twice in PBS. 100 ng/ml LPS was administered to macrophages. Total mRNA was extracted using the TRIZOL extraction kit. 1 µg RNA was retrotranscribed using M-MLV reverse transcriptase minus H in a final volume of 40 µl using the manufacturer's protocol. Amplification of 1 µl cDNA was performed using the following primers: mTNFa forward, 5′-TAGCCAGGAGGGAGAACAGA-3′; mTNFa reverse, 5′-TTTTCTGGAGGGAGATGTGG-3′; bactin forward, 5′-TGTTACCAACTGGGACGACA-3′; and bactin reverse, 5′-GGGGTGTTGAAGGTCTCAAA-3′.

TAMs were purified from tumors as described, and mRNA, obtained as described, was retrotranscribed and amplified by PCR with the following